

Old Dominion University

ODU Digital Commons

Mechanical & Aerospace Engineering Theses & Dissertations

Mechanical & Aerospace Engineering

Fall 1983

Experiments on Melting Around an Isothermal Horizontal Cylinder Under Computer Control

Timothy Moore Rothgeb
Old Dominion University

Follow this and additional works at: https://digitalcommons.odu.edu/mae_etds



Part of the [Heat Transfer, Combustion Commons](#)

Recommended Citation

Rothgeb, Timothy M.. "Experiments on Melting Around an Isothermal Horizontal Cylinder Under Computer Control" (1983). Thesis, Old Dominion University, DOI: 10.25777/6dga-c708
https://digitalcommons.odu.edu/mae_etds/379

This Thesis is brought to you for free and open access by the Mechanical & Aerospace Engineering at ODU Digital Commons. It has been accepted for inclusion in Mechanical & Aerospace Engineering Theses & Dissertations by an authorized administrator of ODU Digital Commons. For more information, please contact digitalcommons@odu.edu.

EXPERIMENTS ON MELTING AROUND AN ISOTHERMAL
HORIZONTAL CYLINDER UNDER COMPUTER CONTROL

By

Timothy Moore Rothgeb
B.S.M.E. December 1981, Old Dominion University

A Thesis Submitted to the Faculty of
Old Dominion University in Partial
Fulfillment of the Requirements for the Degree of
Master of Engineering

Old Dominion University

November, 1983

A. Sidney Roberts, Jr. (Director)

Robert L. Ash

John M. Kuhlman

ABSTRACT
EXPERIMENTS ON MELTING AROUND AN ISOTHERMAL HORIZONTAL
CYLINDER UNDER COMPUTER CONTROL

Timothy Moore Rothgeb
Old Dominion University, 1983
Director: A. Sidney Roberts, Jr.

The melting of a solid around an isothermal horizontal cylinder is a physical phenomenon which must be understood when attempting to design a latent heat storage system. The desire to design such a system is the motivating factor in this research. To gain this understanding of the fundamental melting processes several experiments were designed, and two sets of Stefan and Rayleigh number experiments were undertaken. Experiments were also performed to determine the properties of the paraffin that was used in these investigations. During the investigations of the melting processes, the temperature was measured at several locations throughout the liquid and solid phases. The interface position was also determined photographically at several times during the experiments. These results are compared favorably with recently published numerical solutions to the governing equations. The results also show that both the interface and the temperature field data are symmetric with respect to the vertical gravitational field of force.

ACKNOWLEDGMENTS

The author wishes to thank several people who have assisted him in many ways, including Mr. Richard J. Stenger, Manager, Wax Technology, Suntech Group, who supplied the P-127 paraffin used in these experiments, Mr. William S. Utley, Colorcraft Corp., who supplied the film and photo processing, Helen Sutphen and Rowena Pierce who typed this thesis and Robin Wilkenson who did the graphics. I also would like to thank Dr. A. Sidney Roberts, Jr., who has advised me over the last three years and Ed Cronce, Kent Ferguson, Jerry Robertson and John Schmitt who have aided with the setting up of the laboratory equipment and manufacturing the test cell and enclosure.

Finally, I want to thank Sharon Lee Eisner who has not only offered her friendship and support, but who has done everything from helping with the experiments to typing the rough draft of this thesis. I also want to thank my mother for all she has done.

TABLE OF CONTENTS

	Page
ABSTRACT	
TITLE PAGE	i
ACKNOWLEDGMENTS.....	ii
TABLE OF CONTENTS.....	iii
LIST OF TABLES.....	v
LIST OF FIGURES.....	vi
LIST OF SYMBOLS.....	viii
CHAPTER	
1. INTRODUCTION.....	1
1.1 Problem Statement.....	4
2. DESCRIPTION OF THE THEORETICAL MODEL.....	6
3. EXPERIMENTAL ASSEMBLY AND PROCEDURE.....	12
3.1 Properties of Paraffin.....	16
3.2 Motion of the Melting Interface.....	17
3.3 Temperature Measurements.....	19
3.4 Data Aquisition.....	19
4. DATA ANALYSIS.....	21
4.1 Presentation of Results.....	21
4.1.1. Properties.....	21
4.1.2. Interface Results.....	25
4.1.3. Temperature Field.....	27

CHAPTER	Page
4.2 Discussion of Errors.....	45
4.2.1. Error in the Properties.....	45
4.2.2. Error in the Interface Experiments.....	47
4.2.3. Error in the Temperature Measurements.....	48
5. COMPARISON OF RESULTS WITH THEORY.....	51
5.1 Interface Results Comparisons.....	51
5.2 Temperature Results Comparisons.....	54
6. CONCLUSIONS AND RECOMMENDATIONS.....	61
REFERENCES	63
APPENDIX A: Program Listing for Data Acquisition.....	65
APPENDIX B: Composition of P-127 Paraffin.....	67
APPENDIX C: Instrument Serial Numbers.....	68

LIST OF TABLES

TABLE		PAGE
4.1.	Results of the viscosity experiment.....	22
4.2.	Thermophysical properties of paraffin wax.....	24
4.3.	Coefficient equations for the empirical interface equations.....	27
4.4.	Thermocouple calibration data.....	49
4.5.	Extent of interface misalignment for comparison between experiments with and without thermocouples.....	50
5.1.	Temperature ranges used to develop the experimental isotherms.....	60

LIST OF FIGURES

FIGURE		PAGE
3.1	Experimental set-up.....	13
3.2	Test cell.....	14
3.3	Test cell during experiment.....	15
3.4	Thermocouple locations.....	20
4.1	Density variation with temperature.....	23
4.2	Comparison of four coefficient empirical fit and measured interface position.....	26
4.3	Temperature along line $\theta = 90^\circ$ with empirical interface position, $t = .76$	29
4.4	Temperature along line $\theta = 90^\circ$ with empirical interface position, $t = 2.49$	30
4.5	Temperature along line $\theta = 90^\circ$ with empirical interface position, $t = 4.21$	31
4.6	Comparison of temperature along lines of constant θ to show symmetry, $t = .76$	33
4.7	Comparison of temperature along lines of constant θ to show symmetry, $t = 2.49$	34
4.8	Comparison of temperature along lines of constant θ to show symmetry, $t = 4.21$	35
4.9	Temperature along line $\theta = 90^\circ$, $t = 1.49$	36
4.10	Temperature along line $\theta = 90^\circ$, $t = 4.79$	37
4.11	Temperature along line $\theta = 90^\circ$, $t = 8.11$	38
4.12	Comparison of temperature along lines of constant θ to show symmetry, $t = 1.49$	39
4.13	Comparison of temperature along lines of constant θ to show symmetry, $t = 4.79$	40
4.14	Comparison of temperature along lines of constant θ to show symmetry, $t = 8.11$	41
4.15	Temperature variation with time, $r^* = .33$	43

FIGURE		PAGE
4.16	Temperature variation with time, $r^* = 1.67$	44
4.17	Temperature variation with time, $r^* = 3.67$	46
5.1	Comparison of interface minimum.....	52
5.2	Comparison of interface maximum.....	53
5.3	Comparison of melt volumes.....	55
5.4	Comparison of temperatures along line $\theta = 90^\circ$ at an early time.....	57
5.5	Comparison of temperatures along line $\theta = 90^\circ$ at a late time.....	57
5.6	Isotherm comparison.....	58

LIST OF SYMBOLS

a	cylinder radius, m
C_p	specific heat, KJ/kg°C
g	sea level gravitational constant
h_{SL}	latent heat, KJ/kg
K	thermal conductivity, w/m°C
m	mass, kg
P	nondimensional pressure, $\frac{P^*}{\rho_s (\alpha/a)^2 Pr}$
P_r^*	reduced pressure, r direction, $\bar{P} + \rho_s g_r \bar{r}$
P_θ^*	reduced pressure, θ direction, $\bar{P} + \rho_s g_\theta \bar{r}$
\bar{P}	pressure, Pa
R	interface radius, m
\bar{r}	radius, m
r	nondimensional radius, \bar{r}/a
r^*	nondimensional radius via [11], $(\bar{r} - a)/a$
t	nondimensional time, $\frac{\bar{t}\alpha}{a^2}$
\bar{t}	time, s
T	temperature, °C
\bar{T}	nondimensional temperature, $(\bar{T} - \bar{T}_M) / (\bar{T}_W - \bar{T}_M)$
v	volume, m ³
\bar{V}	velocity, m/s

V nondimensional velocity, $\frac{\bar{v}}{\alpha/a}$

V nondimensional melt volume; melt area/cylinder area

Nondimensional Parameters

Fo Fourier number, $\frac{\bar{t}\alpha}{a^2} = t$

Pr Prandtl number, $\frac{\nu}{\alpha}$

Ra Rayleigh number, $\frac{\text{Pr } g (\bar{T}_w - \bar{T}_M) a^3}{\nu^2}$

Ste Stefan number, $\frac{C_p (\bar{T}_w - \bar{T}_M)}{h_{SL}}$

Greek Symbols

α thermal diffusivity, $\frac{K}{\rho C_p}$, $\frac{m^2}{s}$

β coefficient of thermal expansion, $1/^\circ\text{C}$

η index of refraction

μ viscosity, Pa·s

ν kinematic viscosity, μ/ρ , $\frac{m^2}{s}$

ρ density, $\frac{kg}{m^3}$

$\bar{\phi}$ stream function, m^2/s

θ nondimensional angular coordinate

Mathematical symbols

$\frac{D}{Dt}$	substantial derivative, s ⁻¹
∇^2	Laplacian operator

Subscripts

a	air
M	melt
p	constant pressure
P	paraffin
r	r-direction
s	solid
SL	solid-liquid
w	wall
we	weight
θ	θ-direction

Chapter 1

INTRODUCTION

Melting is of interest in many areas, such as, the formation of the polar ice caps, casting or molding processes, analysis of nuclear reactor accidents, and latent heat energy storage systems. These are a few applications of current interest. Questions about optimal design of latent heat storage systems have motivated the present work, leading to the definition of an experiment task.

The classical treatment of heat transfer during melting assumed that convection was negligible and that the process was pure conduction [1]*. This assumption would only be reasonable if there was no change in the density of the melted liquid as it was heated. It has only been in the last ten to fifteen years that progress toward understanding the basic mechanisms of heat transfer during melting has been made.

Recently, experimental studies [2-7] have examined several geometries that would be of interest in the design of phase change thermal storage and transfer systems. Hale and Viskanta [2] found that for conduction to be the determining factor in melting or freezing that the geometry was very important. In order for conduction to be the controlling factor, the materials would have to be heated from a

*Numbers in brackets refer to the list of references.

horizontal flat plate above the material or cooled from a flat plate below the material. If this situation was reversed, then convection would control the heat transfer. The same authors [3] found, when using a vertical flat plate, that convection dominated the heat transfer process.

Bathelt, Viskanta and Leidenfrost [4,5,6] have been studying the interface motion around single and multiple horizontal cylinders both before the melting interfaces merge and afterwards. By measuring the Nusselt number (both local and average) it has been determined that natural convection plays a major role in the heat transfer process in both the single and multiple tube experiments.

Bathelt and Viskanta [7] have also studied the interface motion during melting and solidification around an axially finned horizontal cylinder. They found that the fins enhanced the melting process much more than the freezing process, and that the orientation of the fins in the gravitational field also has more effect on melting than freezing. The local and average Nusselt numbers for the finned cylinder were within ± 20 percent of those for an unfinned cylinder.

Sparrow, Schmidt and Ramsey [8] have also studied melting around a horizontal cylinder. Their results agree with the results of Bathelt et al. [4-5] even though Sparrow et al. [8] used an eutectic mixture of sodium nitrate and sodium hydroxide as opposed to the paraffin used by Bathelt et al. [4-5].

All of the recent experimental studies have reached the same conclusion that convection cannot be overlooked in order to explain the melting process. Bathelt et al. [4] also concluded that, "theoretical

prediction of the solid-liquid interface position is feasible during the early stages," but once the interfaces of several cylinders merge, it will no longer be possible (i.e. prediction of the interface position around a single cylinder is possible).

Recent numerical analyses have yielded two-dimensional, transient results for the position of melting interface and also for the isothermal and stream function contours. Sparrow, Patankar and Ramadhyani [9] have numerically solved the differential equations (conservation of mass, momentum and energy) using a Boussinesq approximation for a vertical cylinder. The model, which solves for the temperature and streamline fields, clearly shows the importance of convection during the melting process.

Rieger, Projahn and Beer [10] and Prusa and Yao [11] have also provided numerical solutions of the differential equations using the Boussinesq approximation for the horizontal cylinder. Rieger et al. [10] and Sparrow, et al. [9], used a false starting condition to overcome a singularity at time zero. The singularity results because there is no liquid phase before time zero. Prusa and Yao [11] have found a way of removing this singularity. They have also overcome the problem Rieger et al. [10] had where nodal points tended to cluster under a coordinate transformation. Prusa and Yao [11] used a simpler coordinate transformation than used by Rieger et al. [10]. Rieger et al. [10] proposed using a transformation from an x-y rectangular coordinate system to "real space" quasi-cylindrical coordinates. Prusa and Yao started with (r, θ) coordinates and then made the transformation to the "real space," which is much more realistic when melting is occurring about a horizontal tube.

Experimental workers [12,13,14] have also examined how convection effects freezing. Bathelt, Van Buren and Viskanta [12] have studied freezing around a horizontal cylinder. Sparrow et al. [13,14] have studied the freezing problem around a vertical cylinder. The conclusions reached in these studies have been the same, that convection becomes important even when the liquid temperature is only slightly higher than the fusion temperature. It was also found that convection may not only slow the solidification process, but also halt it [13].

1.1 Problem Statement

The numerical solutions of the theoretical model for melting around a horizontal cylinder appear to be well developed, but the experimental verification of these methods is incomplete. Validation of the models and the associated numerical results is important because of the assumptions made in writing the boundary conditions and the governing equations, and also because of the complexity of the numerical algorithms. In particular, experiments would help discover the existence of any possible flow instability. To help bridge this gap, experiments were performed, using paraffin (SUNOCO P-127), aimed at mapping both the temperature field and the interface motion for two different sets of Stefan and Rayleigh numbers with the same Prandtl number. An empirical equation for the interface position was developed for the larger set of Stefan and Rayleigh numbers. The information obtained from these experiments permit comparison of the interface position, the melt volume and the temperature to those reported in the numerical study by Prusa and Yao [11].

In the following chapters the status of the theoretical modeling is described briefly, and experimental results are presented. Where possible the new data is compared with other theoretical and experimental results, and error limits are determined for the data resulting from the current experiments with paraffin.

Chapter 2

DESCRIPTION OF THE THEORETICAL MODEL

This chapter discusses a general theoretical model of the melting process around a circular cylinder. It is included for completeness because the results of these experiments are compared with calculations from models similar to the one presented in this chapter.

The differential equations that describe melting around a horizontal cylinder are derived from the conservation laws of mass, momentum and energy. The following assumptions are made in the derivation of the conservation equations:

- (1) incompressible flow in two dimensions (r, θ) (see Fig. 3.1)
- (2) the Boussinesq approximation [15] (which assumes constant properties except for density in the body force term of the momentum equation and that the acceleration due to gravity is much larger than both the particle acceleration in the vertical direction and the horizontal length scale times the horizontal particle acceleration divided by vertical length scale), and
- (3) the change in density is given by, $\rho_s - \rho = \rho_s \beta (\bar{T} - \bar{T}_M)$.

With these conditions the governing equations in dimensional form are, where over bars denote dimensional quantities:

Continuity

$$\frac{1}{\bar{r}} \frac{\partial(\bar{r} \bar{V}_r)}{\partial \bar{r}} + \frac{1}{\bar{r}} \frac{\partial \bar{V}_\theta}{\partial \theta} = 0 \quad (2.1)$$

Momentum (r-direction)

$$\frac{\bar{D} \bar{V}_r}{\bar{D} \bar{t}} - \frac{\bar{V}_\theta^2}{\bar{r}} = \frac{-1}{\rho_s} \frac{\partial P^*}{\partial \bar{r}} + g_r \beta (\bar{T} - \bar{T}_M) + \nu \left[\bar{\nabla}^2 \bar{V}_r - \frac{\bar{V}_r}{\bar{r}^2} - \frac{2}{\bar{r}^2} \frac{\partial \bar{V}_\theta}{\partial \theta} \right] \quad (2.2)$$

Momentum (θ - direction)

$$\frac{\bar{D} \bar{V}_\theta}{\bar{D} \bar{t}} + \frac{\bar{V}_r \bar{V}_\theta}{\bar{r}} = - \frac{1}{\rho_s \bar{r}} \frac{\partial P^*}{\partial \theta} + \beta g_\theta (\bar{T} - \bar{T}_M) + \nu \left[\bar{\nabla}^2 \bar{V}_\theta + \frac{2}{\bar{r}^2} \frac{\partial \bar{V}_r}{\partial \theta} - \frac{\bar{V}_\theta}{\bar{r}^2} \right] \quad (2.3)$$

Energy

$$\alpha \bar{\nabla}^2 \bar{T} = \frac{\bar{D} \bar{T}}{\bar{D} \bar{t}} \quad (2.4)$$

where, $P_r^* = \bar{P} + \rho_s g_r \bar{r}$, $P_\theta^* = \bar{P} + \rho_s g_\theta \bar{r}$, $\frac{\partial}{\partial \bar{z}} = \frac{\partial^2}{\partial \bar{z}^2} = 0$, and the over bars denote dimensional quantities. Dissipation has been neglected in the energy equation.

The following dimensionless variables and groups are introduced, where the definitions of symbols is further clarified in the list of symbols:

$$r = \frac{\bar{r}}{a}, \quad T = \frac{(\bar{T} - \bar{T}_M)}{(\bar{T}_w - \bar{T}_M)}, \quad P = \frac{P^*}{\rho_s (\alpha/a^2) Pr}, \quad t = \frac{\alpha \bar{t}}{a^2}, \quad V_r = \frac{\bar{V}_r}{\alpha/a}$$

$$V_{\theta} = \frac{\bar{V}_{\theta}}{\alpha/a}, \quad Pr = \frac{\nu}{\alpha}, \quad Ste = \frac{C_p(\bar{T}_w - \bar{T}_M)}{h_{SL}}$$

$$Ra = \frac{Pr g \beta (\bar{T}_w - \bar{T}_M) a^3}{\nu^2}$$

By nondimensionalizing Eqs. (2.1) - (2.4) the following equations result:

Continuity:

$$\frac{1}{r} \frac{\partial}{\partial r} (r V_r) + \frac{1}{r} \frac{\partial V_{\theta}}{\partial \theta} = 0 \quad (2.5)$$

Momentum (r - direction):

$$\begin{aligned} \frac{\alpha^2}{a^3} \left[\frac{DV_r}{Dt} - \frac{V_{\theta}^2}{r} \right] &= g r \beta (\bar{T}_w - \bar{T}_M) T \\ &- \frac{\alpha^2}{a^3} Pr \frac{\partial P}{\partial r} + \frac{\alpha \nu}{a^3} \left[\Delta^2 V_r - \frac{V_r}{r^2} - \frac{2}{r^2} \frac{\partial V_{\theta}}{\partial \theta} \right] \end{aligned}$$

Substituting $(\sin-\theta) g$ for g_r , multiplying by $\frac{a^3}{\alpha \nu}$, and combining terms leads to,

$$\begin{aligned} \frac{1}{Pr} \left[\frac{DV_r}{Dt} - \frac{V_{\theta}^2}{r} \right] &= - \frac{\partial P}{\partial r} + T Ra \sin \theta \\ &+ \left[\nabla^2 V_r - \frac{V_r}{r^2} - \frac{2}{r^2} \frac{\partial V_{\theta}}{\partial \theta} \right] \end{aligned} \quad (2.6)$$

Similarly, for the θ direction,

$$\frac{1}{Pr} \left[\frac{DV_\theta}{Dt} + \frac{V_r V_\theta}{r} \right] = -\frac{1}{r} \frac{\partial P}{\partial \theta} + T Ra \cos \theta + \left[\nabla^2 V_\theta + \frac{2}{r^2} \frac{\partial V_r}{\partial \theta} - \frac{V_\theta}{r^2} \right] \quad (2.7)$$

The normalized energy equation becomes,

$$\alpha \frac{(\bar{T}_w - \bar{T}_M)}{a^2} \nabla^2 T = \frac{(\bar{T}_w - \bar{T}_M) \alpha}{a^2} \frac{DT}{Dt}$$

A final form of the energy equation is obtained by multiplying through by $\left(\frac{a^2}{(\bar{T}_w - \bar{T}_M) \alpha} \right)$, to obtain

$$\nabla^2 T = \frac{DT}{Dt} \quad (2.8)$$

It should be noted that a general nondimensionalization has been done here to show the importance of certain key nondimensional parameters. Furthermore, the numerical studies of references [9-11] have all made some kind of coordinate transformations presenting their results in a variety of nondimensional radial coordinates.

Finally, another equation is needed to describe the interface position, R , which is non-orthogonal to the radius vector in the $(r-\theta)$ coordinate system. This equation is the energy balance at the interface. Assuming that heat conduction is everywhere normal to the interface and is just balanced by the heat of fusion, the energy balance becomes:

$$\frac{\partial R}{\partial \bar{t}} = \frac{-k_L}{\rho_S h_{SL}} \left(\frac{\partial \bar{T}}{\partial r} - \frac{1}{R^2} \frac{\partial R}{\partial \theta} \frac{\partial \bar{T}}{\partial \theta} \right)_{\bar{r} = R}$$

Reduction to dimensionless form yields,

$$\left(\frac{\partial r}{\partial t}\right)_{r=R/a} = -Ste \left[\frac{\partial T}{\partial r} - \frac{1}{r^2} \frac{\partial r}{\partial \theta} \frac{\partial T}{\partial \theta} \right]_{r=R/a} \quad (2.9)$$

where R is the interface radius and a is the heated cylinder radius.

This is the same energy balance reported by Prusa and Yao [11].

The $\partial r/\partial \theta$ term arises from the fact that the interface is not necessarily a circle about the origin of the coordinate system.

Therefore, rays of constant θ are not always perpendicular to the interface.

The remaining boundary conditions are the conventional ones for convection heat transfer [15]. The boundary and initial conditions for temperature are:

$$\begin{aligned} T &= 1 ; r = 1 \quad t > 0 \\ T &= 0 ; r = R/a \quad t > 0 \end{aligned} \quad (2.10)$$

The boundary and initial conditions for velocity at the cylinder are:

$$\begin{aligned} V_r &= V_\theta = 0 ; r = 1, \quad t > 0 \\ &(\text{no slip, no penetration}) \end{aligned}$$

The boundary conditions for velocity at the moving interface are derived by introducing the stream function and relating it to the velocity. The stream function is defined by

$$\bar{V}_r = \frac{1}{r} \frac{\partial \bar{\psi}}{\partial \theta} \quad \bar{V}_\theta = -\frac{\partial \bar{\psi}}{\partial r}$$

where $\bar{\psi}$ is the dimensional stream function. Since the interface is a stream line, the stream function is a constant at the interface. Therefore, the differential of the stream function at the interface is zero.

$$d\bar{\psi} = 0 = \frac{\partial \bar{\psi}}{\partial \bar{r}} d\bar{r} + \frac{\partial \bar{\psi}}{\partial \theta} d\theta + \frac{\partial \bar{\psi}}{\partial \bar{t}} d\bar{t}$$

substituting for $\frac{\partial \bar{\psi}}{\partial \bar{r}}$ and $\frac{\partial \bar{\psi}}{\partial \theta}$ leads to,

$$0 = -\bar{V}_\theta d\bar{r} + \bar{r} \bar{V}_r d\theta + \frac{\partial \bar{\psi}}{\partial \bar{t}} d\bar{t}, \quad \text{at } \bar{r} = R$$

The $\partial \bar{\psi} / \partial \bar{t}$ term is related to the interface motion and can be solved for by use of Eq. (2.9). This is the boundary condition at the interface for velocity and together with the boundary conditions at the cylinder wall, the total boundary conditions for velocity are:

$$\bar{V}_r = \bar{V}_\theta = 0; \quad r = 1 \quad t > 0$$

$$0 = -\bar{V}_\theta d\bar{r} + \bar{r} \bar{V}_r d\theta + \frac{\partial \bar{\psi}}{\partial \bar{t}} d\bar{t}, \quad \text{at } \bar{r} = R \quad (2.11)$$

Equations (2.5)-(2.9) and boundary conditions as given by Eqs. (2.10) and (2.11) constitute the transient, non-linear model of the melting experiment.

The complexity of these equations and boundary conditions is part of what has led to the involved numerical solutions, which should be verified by experiments. The results of the numerical analyses reported in [10,11] have been compared with the results of the present experiments in later chapters.

Chapter 3

EXPERIMENTAL ASSEMBLY AND PROCEDURE

The experimental set-up for the temperature and interface motion experiments is shown in Fig. 3.1. Two different test cells were used in obtaining the interface motion and temperature field data for the larger values of Stefan and Rayleigh numbers. A general perspective and a photograph of the test cell during a representative experiment are shown in Figs. 3.2 and 3.3 respectively. The only differences in the two test cells are that the cell used to gather the interface data has, (1) a glass back plate as contrasted to the aluminum back plate used in the temperature runs, (2) a sealing ring around the central cylinder which was eliminated in the temperature runs, and (3) a wooden cell body as opposed to an aluminum cell body. The test chamber was made from plywood with glass windows front and back for viewing the test cell. The lights in the test chamber serve a dual purpose, to provide a source of light for taking photographs and as a source of heat for maintaining the environment temperature around the test cell close to the paraffin fusion point. A 35mm camera was used to photograph the test cell during the experiment in order to locate the interface in space and time, and to detect any flow disturbance caused by the insertion of the thermocouples into the paraffin.

The properties for some pure paraffins are very well known. But, since paraffin is a generic name for a large group of hydrocarbons with

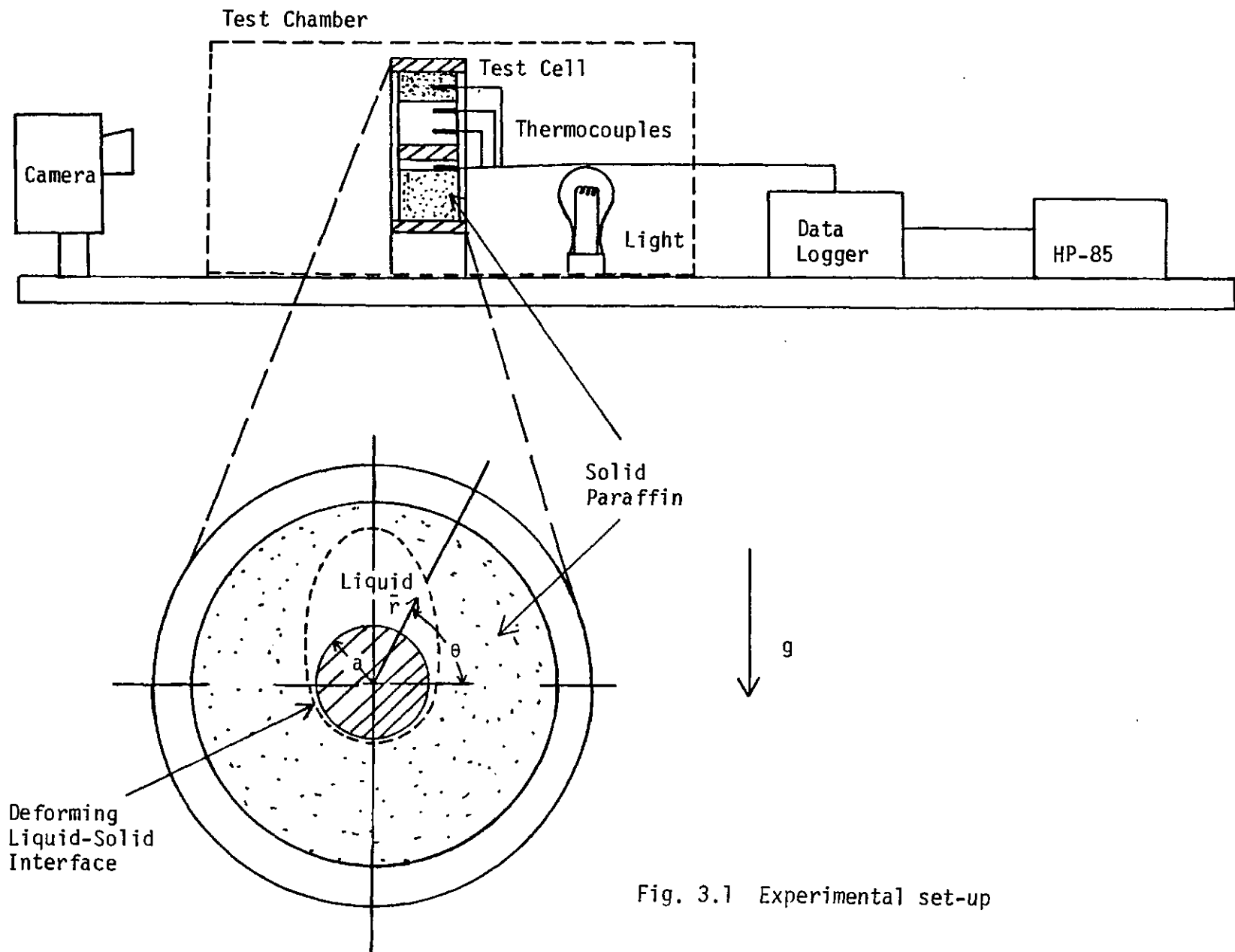


Fig. 3.1 Experimental set-up

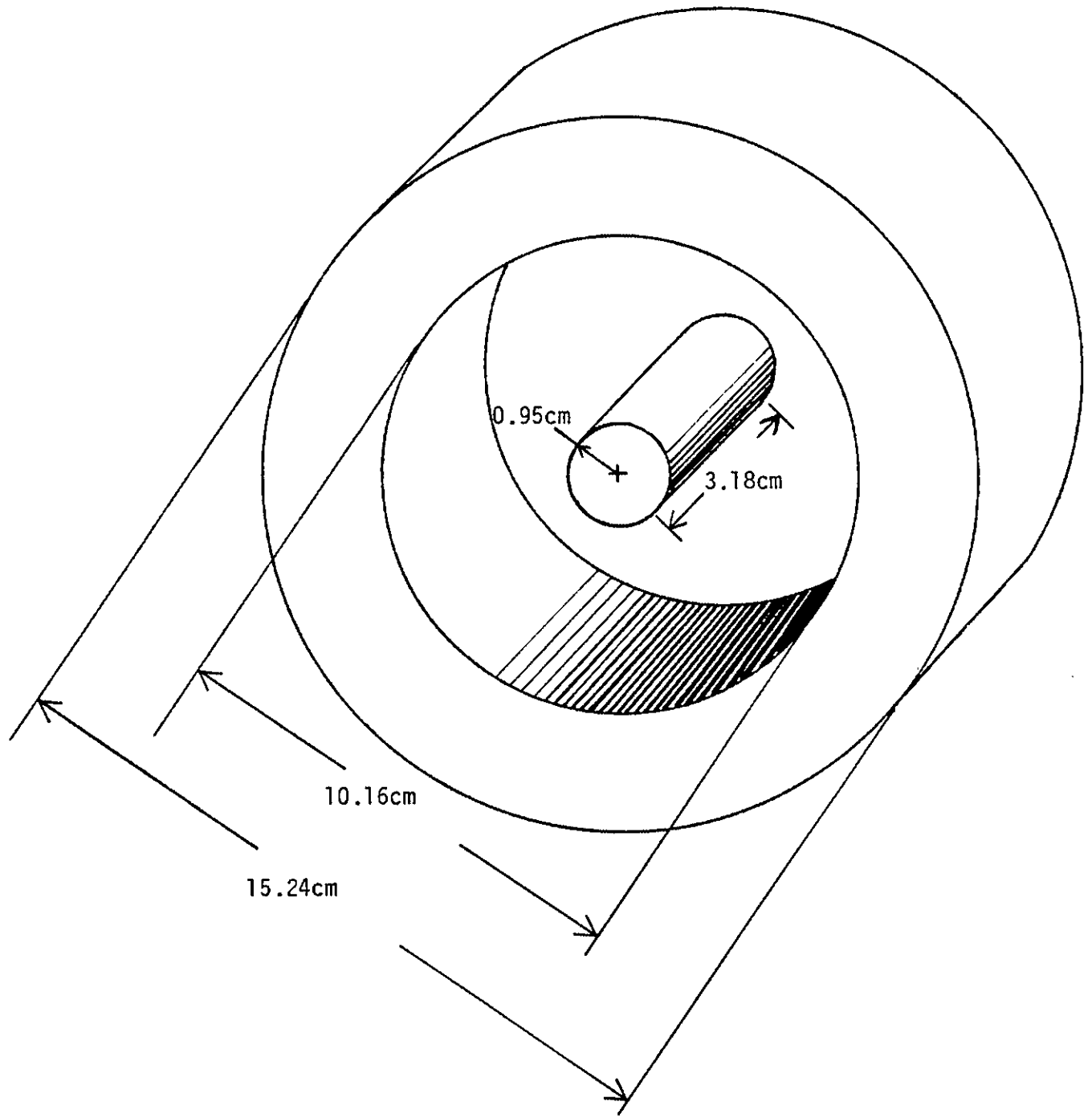


Fig. 3.2 Test cell

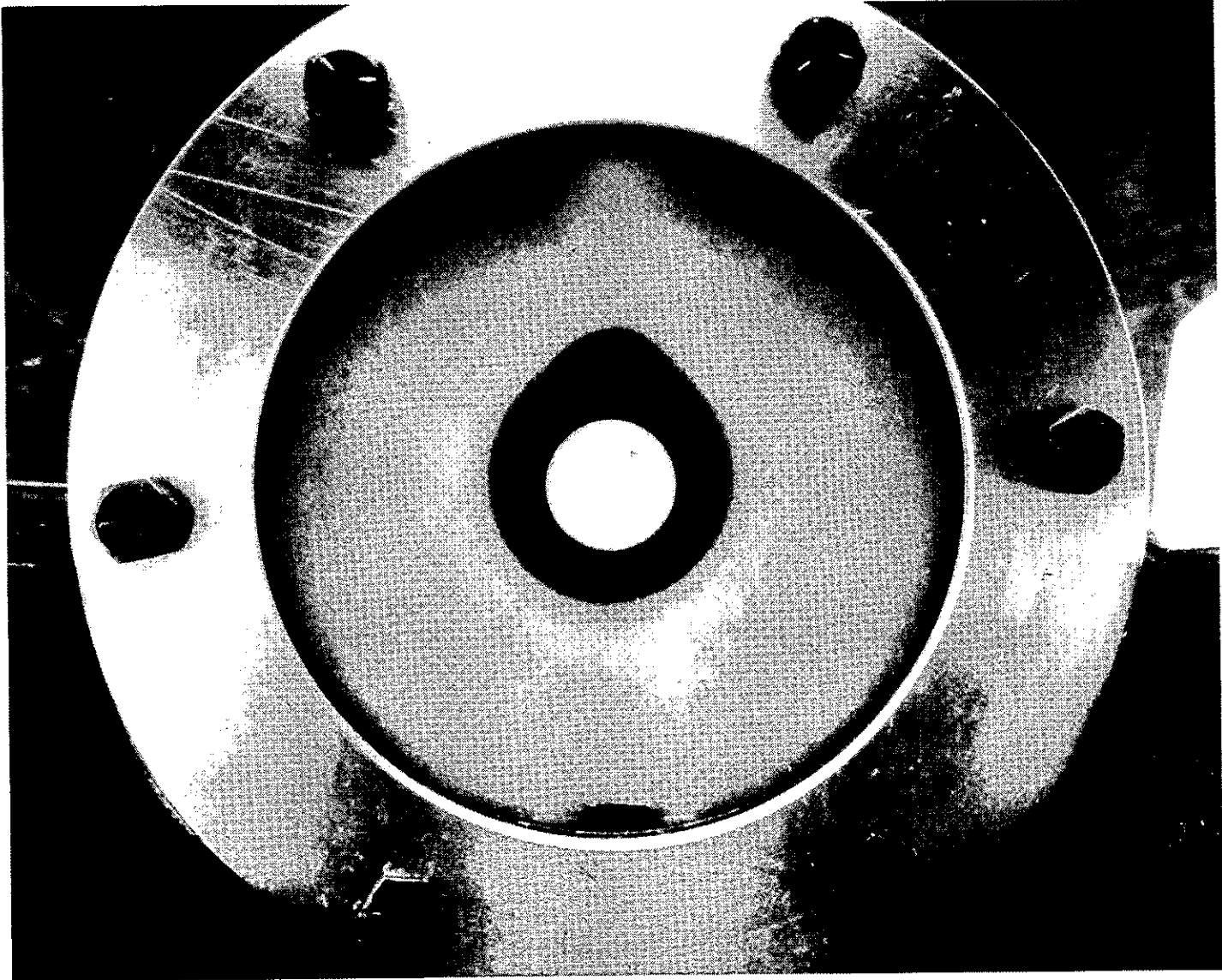


Fig. 3.3 Test cell during experiment

the general chemical formula of C_nH_{2n+2} ; the properties for all paraffins and paraffin mixtures are not well known. In these experiments a mixture of paraffins, known as SUNOCO P-127 was employed. Because of a possible variation in the mixture composition, it was felt that density and viscosity of the P-127 used in the present work should be measured. Density and viscosity were chosen because of their significance in Eqs. (2.5) - (2.9) as given in Chap. 2.

Two different assemblies were used to determine the density and viscosity of the paraffin (SUNOCO P-127). The viscosity was measured using a saybolt viscometer with universal orifice. The density was measured by suspending a volume of known weight in the paraffin.

The following sections describe the procedures used for determining the properties of paraffin, the interface motion, the temperatures throughout the melt, and the data acquisition system used in gathering the temperature data.

3.1 Properties of Paraffin

The kinematic viscosity was deduced using a Saybolt viscometer. The first step in using the viscometer was to fill it with the P-127. The temperature of both the viscometer and the paraffin sample were then brought to equilibrium at 15.6°C (28.0°F) above the melt temperature of the P-127. The paraffin is then released and flows through a standard orifice into a flask with a graduation mark at 60 ml. The time to fill the flask to the graduation mark can be converted to m^2/s using an equation given in Baumeister et al. [19]. This experiment was performed four times and the average of the Saybolt seconds was taken as the viscosity. The results are reported in Chap. 4.

The density was measured using Archimedes Principle. This was done by raising the temperature of the paraffin, which was submerged in a constant temperature bath, from 57.8°C (136.°F) to 88.1°C (190.6°F) in steps of approximately 3.3°C (6.0°F). A brass weight of known volume was suspended in the P-127 and when equilibrium was reached at each temperature step it was weighed and the density and coefficient of thermal expansion were calculated from a static force balance. The density at the lowest temperature was 814.6 Kg/m³ (50.85 lbm/ft³) and the coefficient of thermal expansion β , was 7.95×10^{-4} 1/°C (4.42×10^{-4} 1/°F). For complete results see Chap. 4 and Fig. 4.1. It should be noted that the importance of β is indicated in Eqs. (2.2) and (2.3) or through its relationship to the Rayleigh number in Eqs. (2.6) and (2.7).

3.2 Motion of the Melting Interface

The interface motion was mapped for two different sets of Stefan and Rayleigh numbers ($Ste = .18$, $Ra = 1.5 \times 10^5$; $Ste = .10$, $Ra = 8.8 \times 10^4$) with the same Prandtl number, $Pr = 52$. Three melt experiments were planned, two employing both sets of Stefan and Rayleigh numbers without thermocouples inserted into the test cell, and one experiment at the lower set of values with the thermocouples inserted. This was done to determine the effect of the thermocouples on the interface motion by photographic comparison. The procedure for following the interface motion was basically the same for each case with distinction between runs being due only to the presence of the thermocouples and the duration of the tests.

For each experiment the first step was to raise the temperature of the test chamber and the test cell (which had been filled with P-127 paraffin) to a temperature of approximately 53.3°C (128.0°F), which is 2.2 degrees celsius below the melt temperature of the paraffin. This was done by turning on the lights in the test chamber and using the Fluke data logger to control the air temperature by automatically switching power to the lights to maintain thermal equilibrium. Once equilibrium was reached the temperature of the central cylinder was brought quickly up to a constant temperature (which established the desired Stefan and Rayleigh numbers) in either one of two ways. Either an electric cartridge heater with the Fluke data logger controlling the temperature or water being pumped from a constant temperature bath was used to raise the central cylinder temperature. The cartridge heater was used in the interface experiments with the higher set of Stefan and Rayleigh numbers. The constant temperature bath was used in the experiments with the lower set of Stefan and Rayleigh numbers. The motion of the interface was then recorded by taking 35mm slides every five minutes for the duration of the test (50 minutes for the higher set and 100 minutes for the lower set of Stefan and Rayleigh numbers). After the slides of the interface were developed the interface was projected (at approximately twice the actual size) onto polar graph paper, traced and measured every ten degrees around the cylinder to the nearest $1/40$ of an inch. (Note: The interface for the lower set of Stefan and Rayleigh numbers was only measured at 0° and 180° as reported in later chapters).

3.3 Temperature Measurements

The temperature was measured in the liquid and solid phases at 26 points on the mid-plane of the test cell as indicated in Fig. 3.4, using 30 gauge (0.010 inch diameter) iron-constantan thermocouples. The thermocouples were inserted horizontally into the test cell to positions on a mid-plane which was normal to the axis of the heated cylinder. The temperatures were detected by a Fluke 2200B data logger and were recorded periodically by an HP-85 micro-computer.

3.4 Data Acquisition

The temperature data for these experiments was gathered directly by an HP-85 micro-computer linked (via an HP-IB bus) to a Fluke 2200B data logger. To gather the data, the data logger was set in the continuous scan mode at the fast speed (15 readings per second). Once equilibrium was reached at 53.3°C (128.0°F), the temperature of the central cylinder was quickly increased to the desired temperature for that data set (e.g., by pumping water from a constant temperature bath through it), and the computer was activated. Once activated, the computer scanned the channels until it found the last channel. At that moment the time signal, which the Fluke broadcasts before each scan, along with one set of temperatures were recorded. The computer then waited for a preset interval, which was determined for each experimental run, and then repeated the process. Data was gathered at 50 different times. A program listing is given in Appendix A. Software was created which reduced the data to a non-dimensional form for presentation.

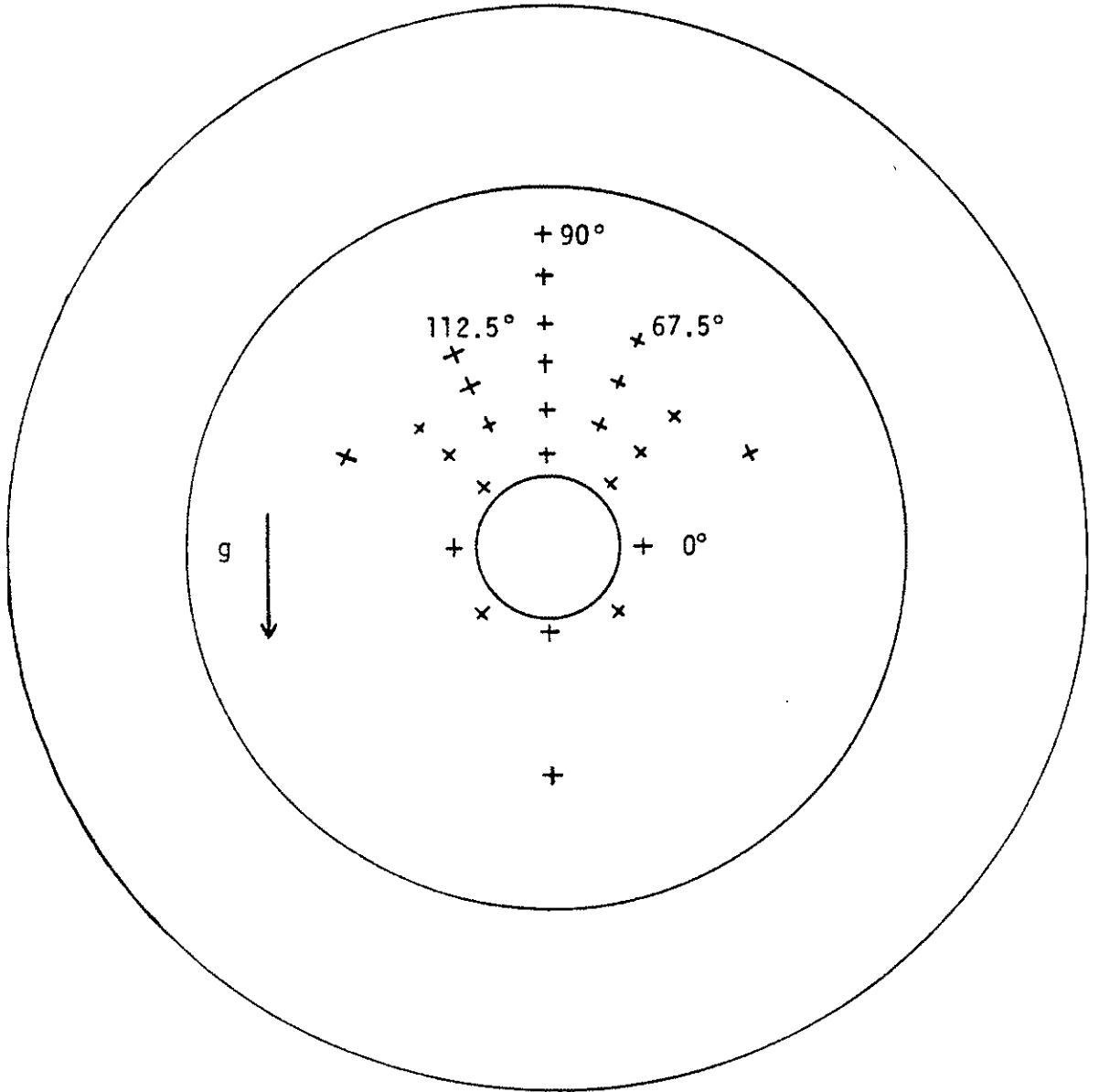


Fig. 3.4 Thermocouple locations

CHAPTER 4

DATA ANALYSIS

This chapter presents the results of the experiments done for this study. The results are presented in two sections. The first section presents the data that was measured. In the second section sources of error and differences between calculated and measured values are discussed, and these errors are quantified.

4.1 Presentation of Results

The results are presented in three parts, the measured properties of the P-127 paraffin, the interface motion and the time-dependent temperature distributions. As discussed in Chap. 3, two properties were measured, density and viscosity. The index of refraction was measured by [17] and these values are also reported.

4.1.1 Properties

The density was measured indirectly using Archimedes Principle as described in Chap. 3. Since a mass balance was used to measure the force to support the weight, the gravity term can be divided out, to leave a mass that is proportional to the force needed to support the weight, in either the air or the paraffin. The density is then calculated by the difference between the mass in the air and the mass in the paraffin divided by the volume of the weight $((m_a - m_p)/v_{we})$. The densities found by this method are shown along with a least squares

curve fit in Fig. 4.1 This graph shows that the density varies linearly over the temperature range measured. This linear relationship is important because the coefficient of thermal expansion was assumed constant in the governing equations (i.e., the measured linear relationship was assumed correct over the temperature range of interest).

The kinematic viscosity of the P-127 paraffin was measured in a Saybolt viscometer as described in Chap. 3. The viscosity data is shown in Table 4.1 along with the average of the Saybolt seconds (sus). This average was converted to m^2/s using the following equation from Baumeister et al. [19]:

$$1 \times 10^{-4} [.00226 (\text{sus}) - 1.95 / (\text{sus})] = \frac{\text{m}^2}{\text{s}} \quad (4.1)$$

Table 4.1 Viscosity experiment results

	Temperature (°C)	Time (sus)
	71.1	47.37
	71.1	44.52
	71.1	46.24
	71.1	45.20
Average	71.1(160.0°F)	45.8

The kinematic viscosity, using Eq. (4.1) and based on the average above, was found to be $\nu = 6.10 \times 10^{-6} \text{ m}^2/\text{s}$ with a standard deviation of $4.0 \times 10^{-7} \text{ m}^2/\text{s}$.

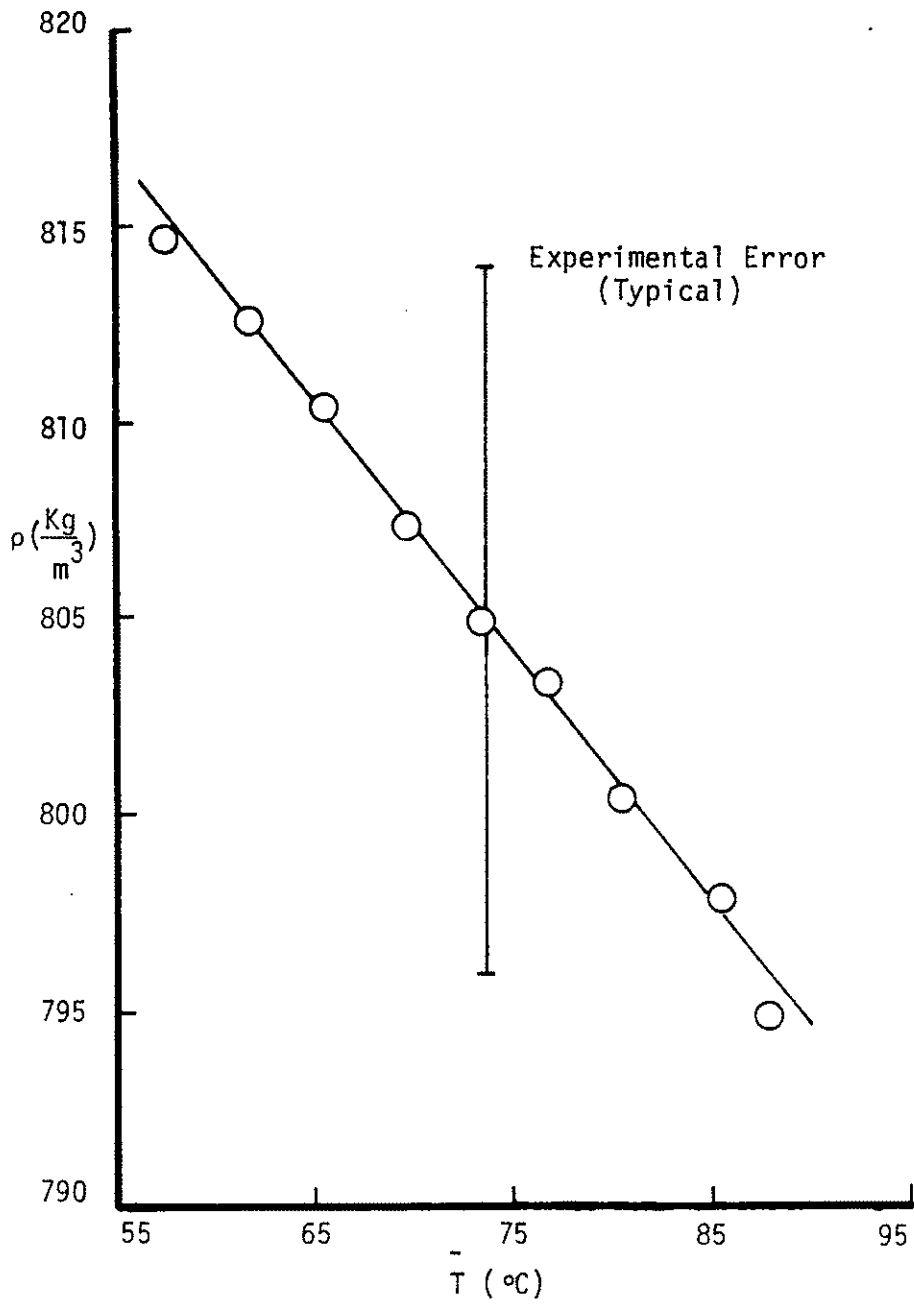


Fig. 4.1 Density variation with temperature

Although the index of refraction is not needed in these experiments, it was anticipated that the values measured by R. J. Stenger [17] might be used for reference in future experiments. The index of refraction measured using sodium-D light was found to be, $n = 1.4205$ at 65.6°C (150.0°F) and $n = 1.4205$ at 98.9°C (210.0°F). The theory of the index of refraction is described by Born and Wolf in [18].

The values for specific heat, thermal conductivity and latent heat were taken to be those reported by Haji-Sheikh et al. [16], on the advice of R. J. Stenger [17] (See table 4.2).

Table 4.2 Thermophysical properties of paraffin wax*

Specific heat of solid	2.95	KJ/kg $^{\circ}\text{C}$
Density of solid	818	Kg/m 3
Density of solid (current work)	816.6	Kg/m 3
Thermal conductivity	0.24	w/m $^{\circ}\text{C}$
Heat of fusion	226	KJ/kg
Viscosity	4.90×10^{-6}	m 2 /s
Viscosity (current work)	6.10×10^{-6}	m 2 /s

*This information was obtained from reference [16] except as noted.

4.1.2 Interface Results

The interface data were gathered in three experiments as described in Chap. 3. The data gathered in the experiments with the higher set of Stefan and Rayleigh numbers was used in developing an empirical equation for the interface radius. The first step in developing the empirical equation was to pick an (r, θ) function that would fit the data. A trigonometric function of the form

$$R = A_0 + A_1 \sin \theta + A_2 \sin^2 \theta + A_3 \cos(2\theta) + A_4 \cos^2(2\theta) \quad (4.2)$$

was chosen. The values of these trigonometric functions were calculated every ten degrees around the cylinder and entered into a 36 x 5 matrix (A) of multipliers. This matrix is equal to the data at each time, which forms a 36 x 1 matrix (B). Inverting the 36 x 5 matrix (A^{-1}) and multiplying both sides by this matrix ($A^{-1} A = A^{-1} B$) reduces the matrices to a 5 x 5 and a 5 x 1. This is then solved, using a computer, to determine the coefficients at each time. A least squares curve fit was used to obtain an equation of each coefficient with time. When this was done the equation showed an irregular dependence on A_4 . The $\cos^2(2\theta)$ term was dropped because of this and the four remaining coefficients were calculated again. The equations obtained for the coefficients were then recalculated. The equations obtained for the coefficients are shown in Table 4.3 where the interface radius is given in inches, the time is in minutes and the angle is measured from the horizontal right (positive x-axis) in degrees. Figure 4.2 shows the 4 coefficient fit along with the experimental data.

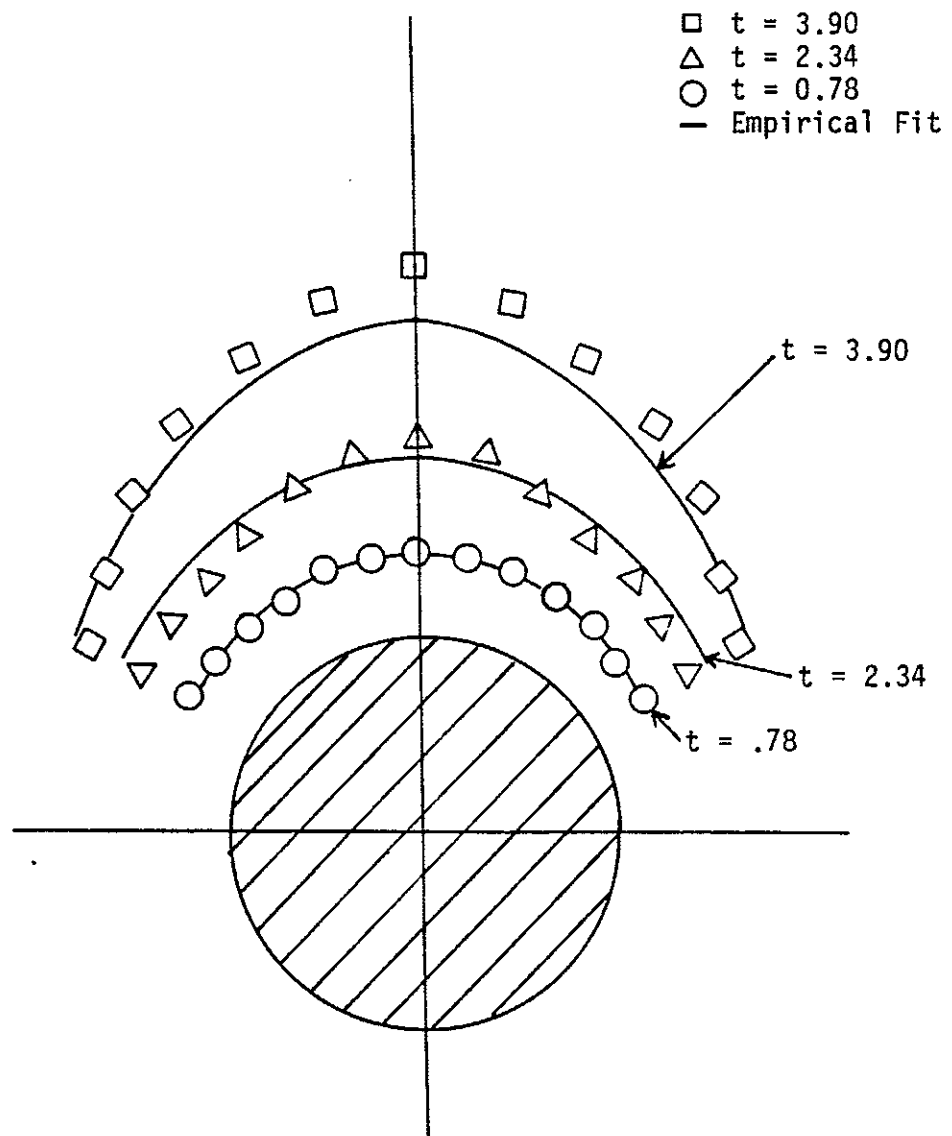


Fig. 4.2 Comparison of 4 coefficient empirical fit and measured interface position

Table 4.3 Coefficient equations for the empirical fits

Coefficient	5 Coefficient fit	4 Coefficient fit
A_0	$.375 + .040\bar{t}^{.517}$	$.375 + .040\bar{t}^{.524}$
A_1	$5.0 \times 10^{-5}\bar{t}^{2.010}$	$4.837 \times 10^{-5}\bar{t}^{2.082}$
A_2	$2.882 \times 10^{-5}\bar{t}^{1.963}$	$2.067 \times 10^{-5}\bar{t}^{2.060}$
A_3	$-2.882 \times 10^{-5}\bar{t}^{1.963}$	$-2.067 \times 10^{-5}\bar{t}^{2.060}$
A_4	$2.40 \times 10^{-3} + 3.24 \times 10^{-4}\bar{t}$	*****

The remaining interface experiments provide two things: (1) a Stefan number that is identical to one of the Stefan numbers that results were reported for in references [10 & 11], and (2) a way of determining the effect of the thermocouples that were inserted for the temperature experiments. The comparisons of this data with the results of [10 & 11] are presented in Chap. 5. The effect of the thermocouples is discussed later in this chapter.

4.1.3 Temperature Field

The temperature was measured at 26 locations throughout the paraffin as shown on Fig. 3.4. Once the data had been entered into the HP-85 micro-computer as described in Chap. 3, software was created to nondimensionalize and store the temperature matrix.

The data obtained in the temperature experiments gives an approximate interface position, a measure of symmetry and the distribution of the temperature field. The temperature field is used to plot isotherms which are compared in Chap. 5 with those reported by Prusa and Yao [11].

Figures 4.3 through 4.5 show the mean* nondimensional temperature at vertical (90°) along with the interface position as predicted by the four coefficient empirical equation (note: a nondimensional temperature of zero would indicate the interface being located at this position). This data is for the larger set of nondimensional parameters; $Ste = 0.18$, $Ra = 150,000$.

Figure 4.3 shows that the interface position as predicted by both the empirical equation and the temperature for time $t = .7635$, lies between the first and second thermocouple positions. Figures 4.4 and 4.5, which are at later times, do not show as good a correspondence between the interface position predictions. The temperatures suggest a range in which the interface could lie.

The size of the standard deviations shown in Figs. 4.3 through 4.5 seems to depend on where the thermocouple is located. When the thermocouple is located either in the solid or away from the interface, the standard deviation is small. These small standard deviations give a base accuracy of the equipment and procedure used to make the temperature measurements. When the thermocouple is located in the transition region (near the interface) the standard deviation is much

*Mean values are determined from multiple runs.

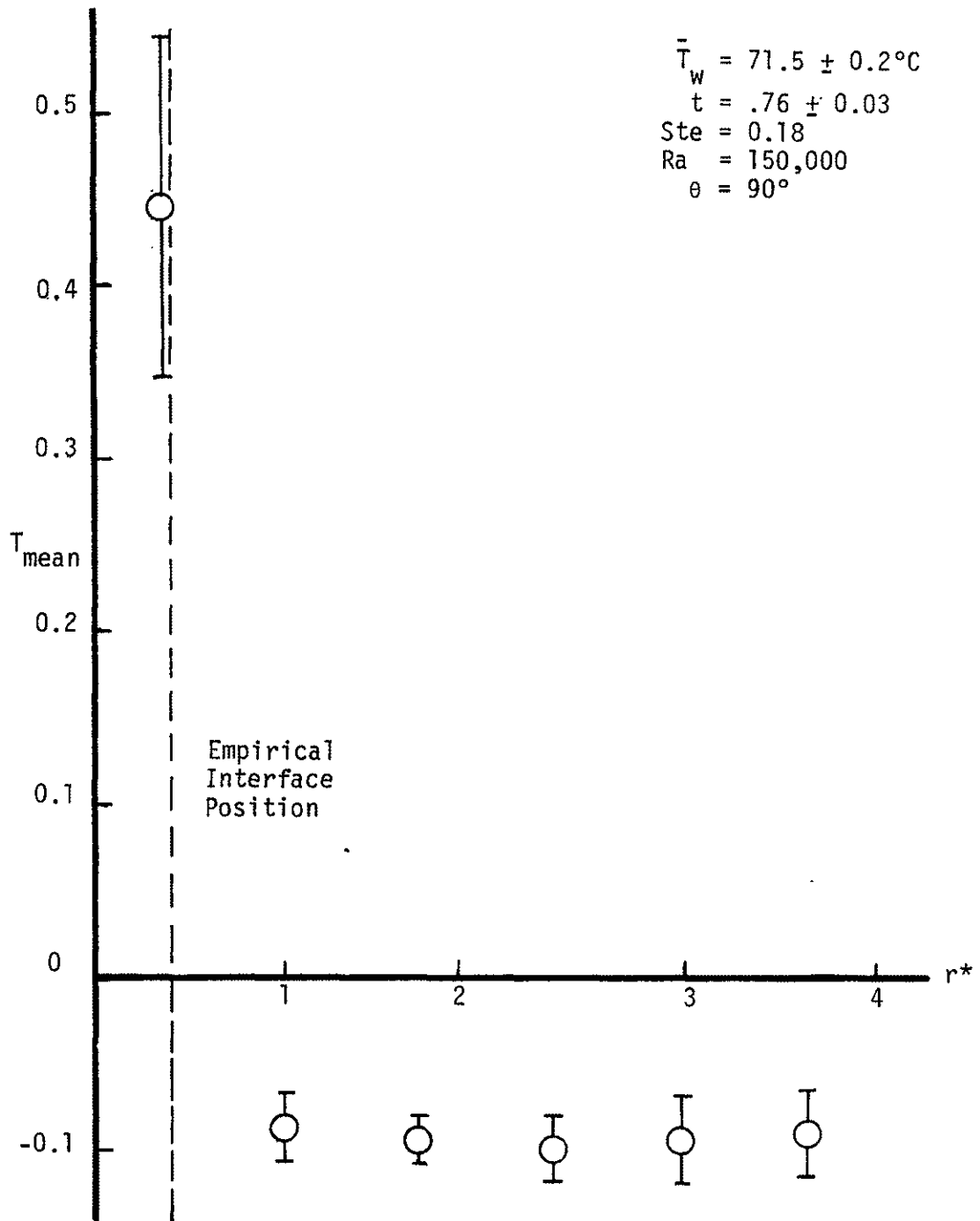


Fig. 4.3 Temperature along line of constant θ with empirical interface position, $t = .76$

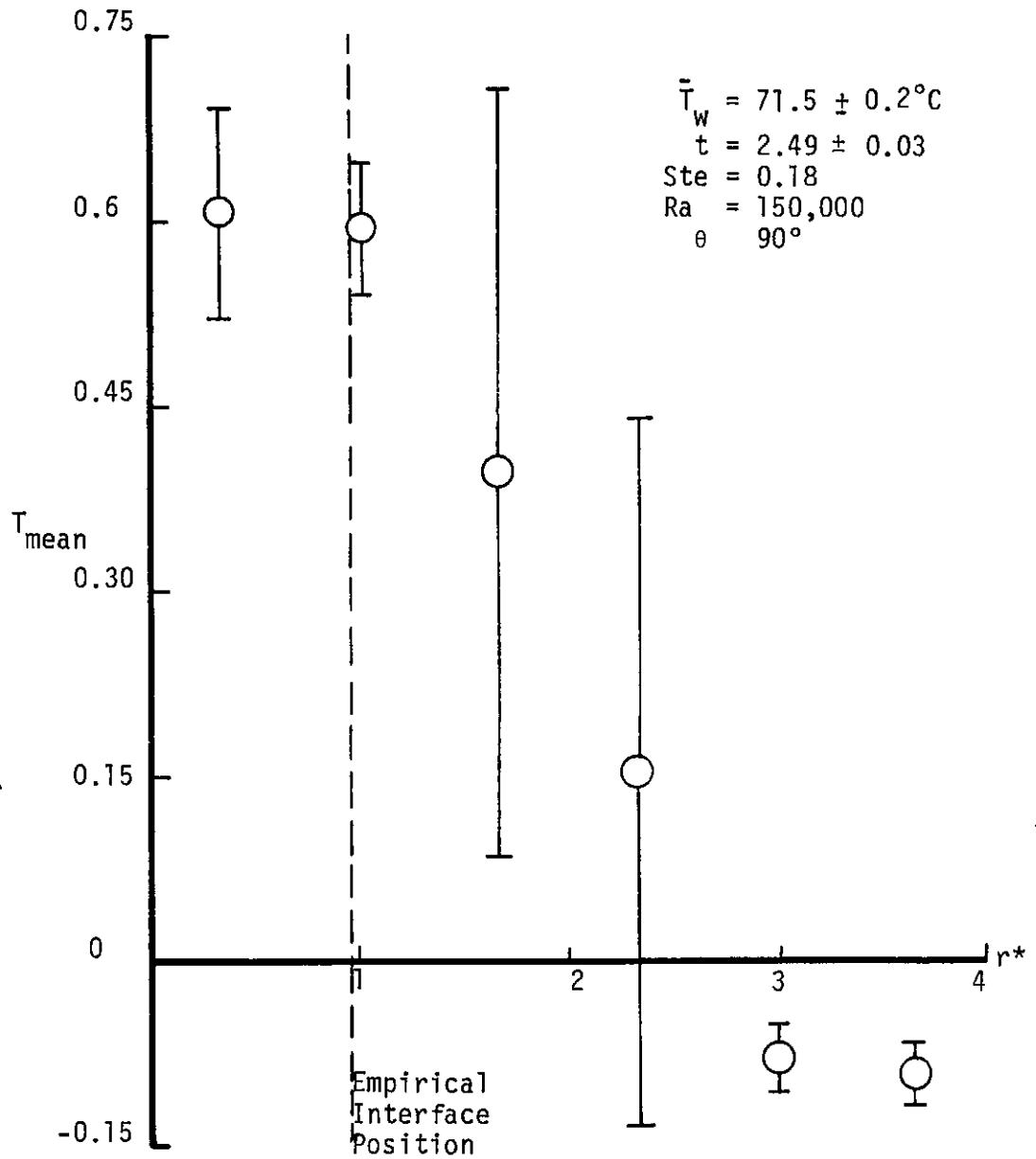


Fig. 4.4 Temperature along line $\theta = 90^\circ$ with empirical interface position, $t = 2.49$

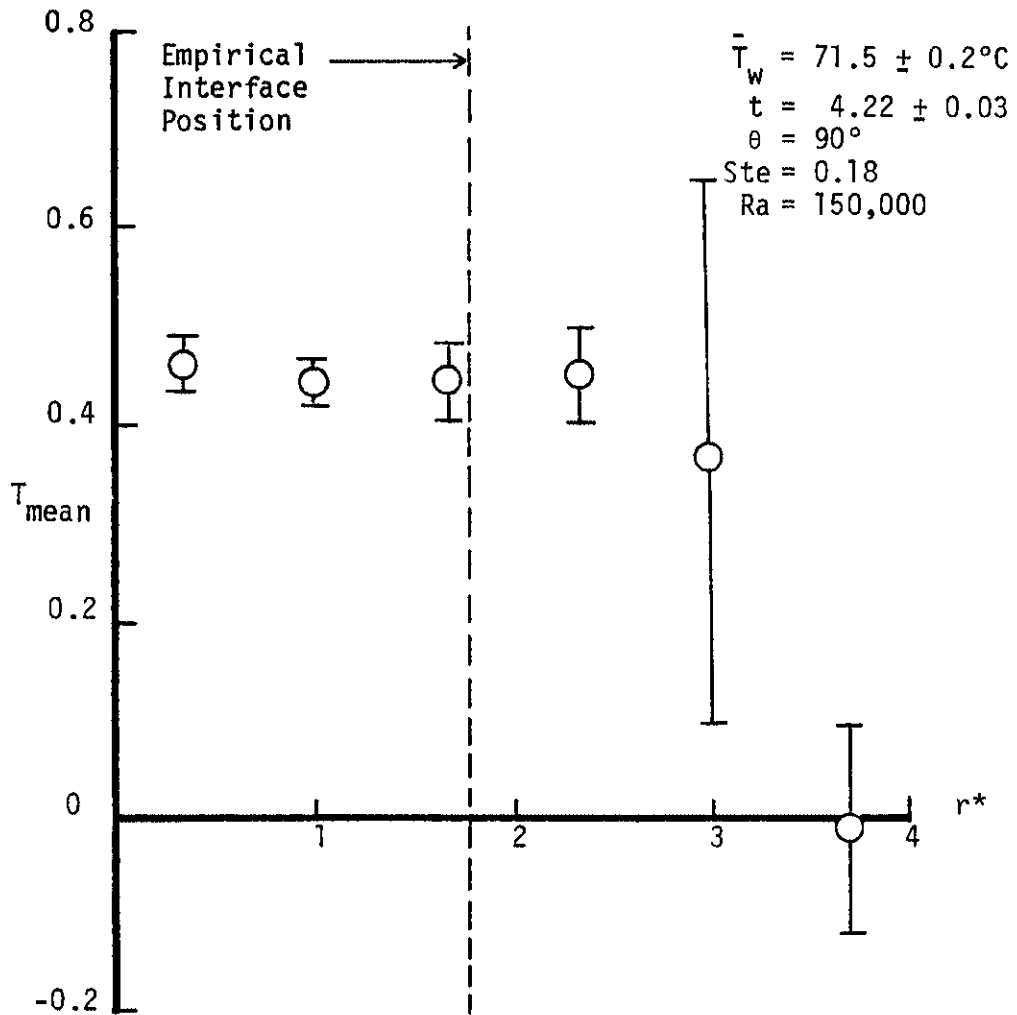


Fig. 4.5 Temperature along line $\theta = 90^\circ$ with empirical interface position, $t = 4.22$

larger. This large standard deviation is due to the difficulty of reproducing the exact same conditions and the transient nature of this region.

Figures 4.6 through 4.8 show the mean nondimensional temperatures and the predicted interface position for $\theta = 67.5^\circ$ and $\theta = 112.5^\circ$ at three times. This is shown to give a measure of the symmetry in the temperature field about the vertical (gravity) axis. Once again the trend in the standard deviations is the same as described above.

The same general trends may be seen in Figs. 4.9 through 4.11 for the lower Rayleigh and Stefan numbers except that the time scale has been expanded. Again, the earlier times show a much smaller range of possible locations of the interface based on the temperature measurements.

The symmetry of the temperature field for the lower set of nondimensional parameters is shown in Figs. 4.12 through 4.14 with results being similar to those found for the higher set of parameters (Ra and Ste).

The standard deviations for this lower set of parameters show the same trend of being large in the transition region and small in both the solid and at times long after the interface has passed.

In general, the standard deviations of the temperatures are small both in the solid and well after the interface passes, and become very large in the transition region. This is because of the difficulty in reproducing the exact convective transport conditions. The uncertainty is due in large part to transient behavior in this region (i.e. the melting at the interface and the convective flow which changes rapidly at or near the interface).

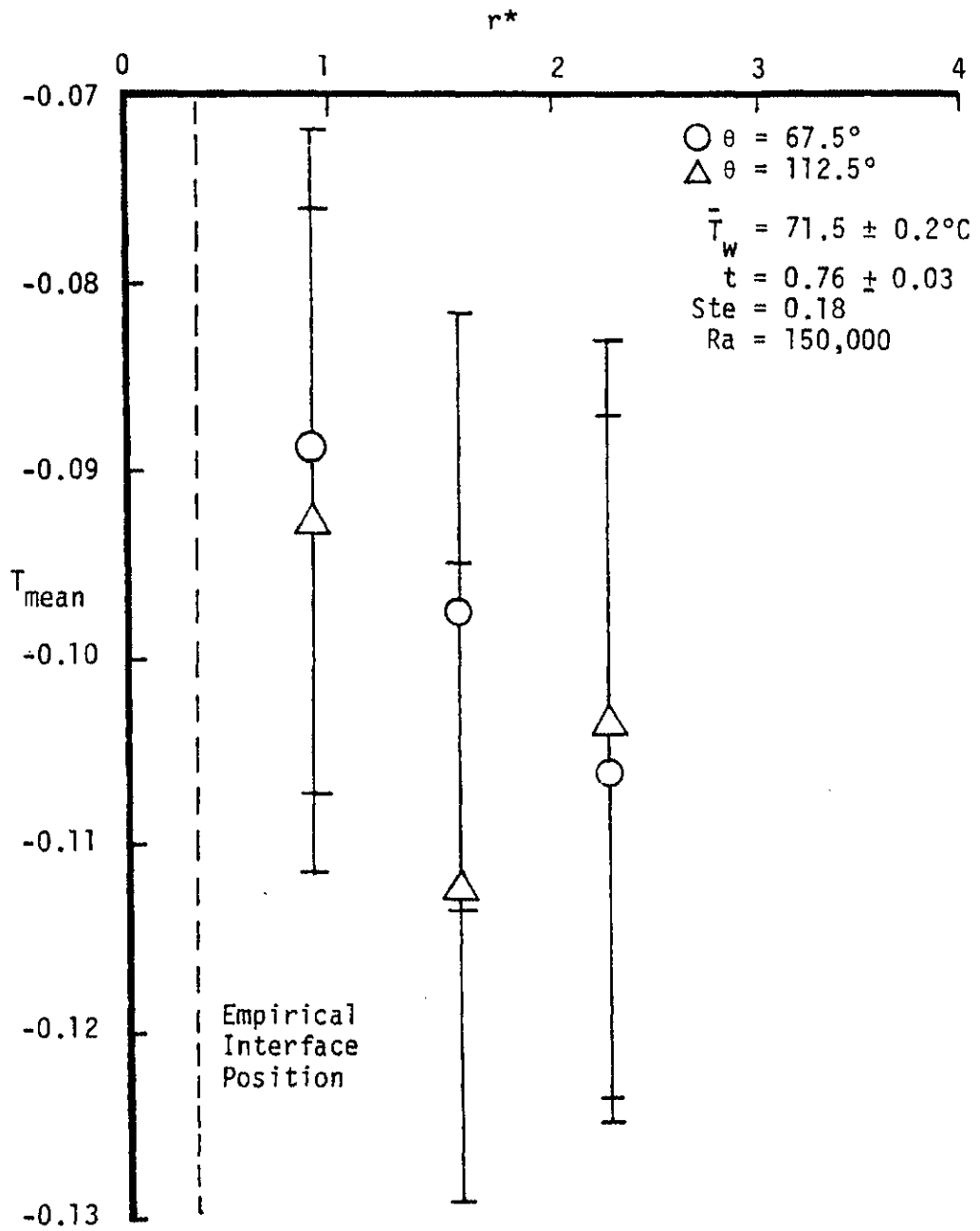


Fig. 4.6 Comparison of temperature along lines of constant θ show symmetry, $t = 0.76$

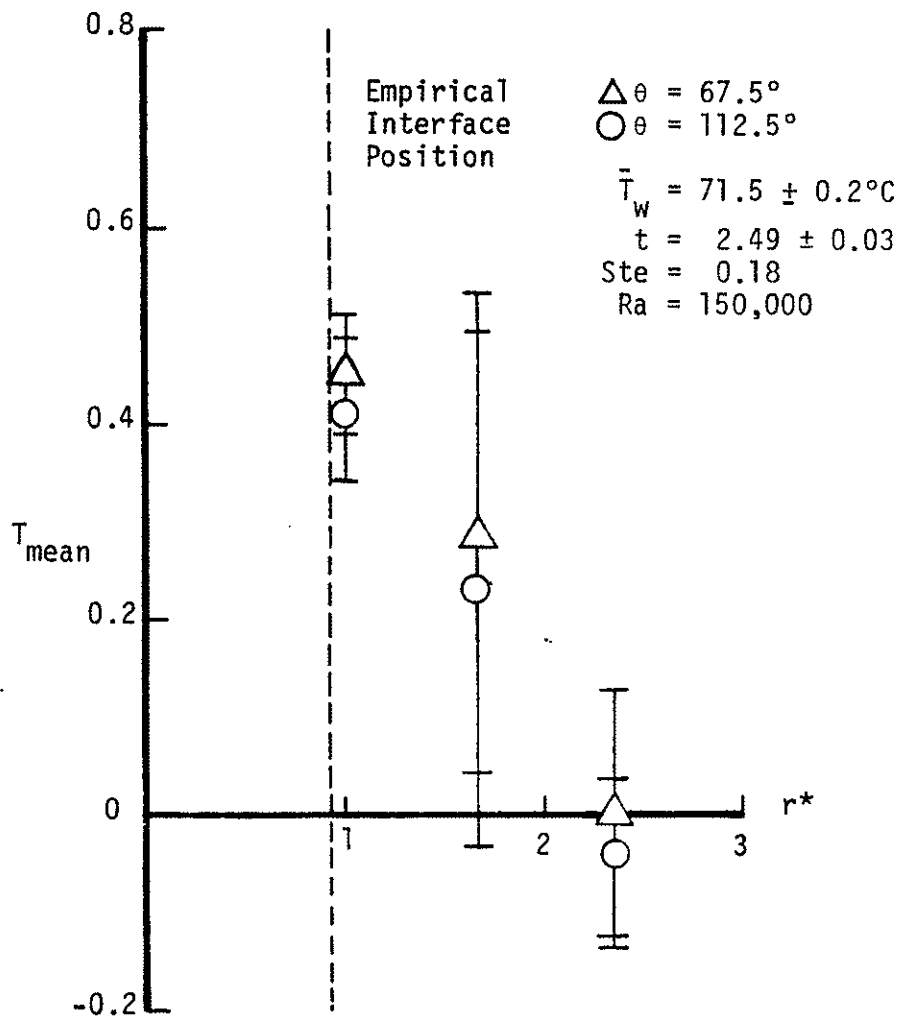


Fig. 4.7 Comparison of temperature along lines of constant θ to show symmetry, $t = 2.49$

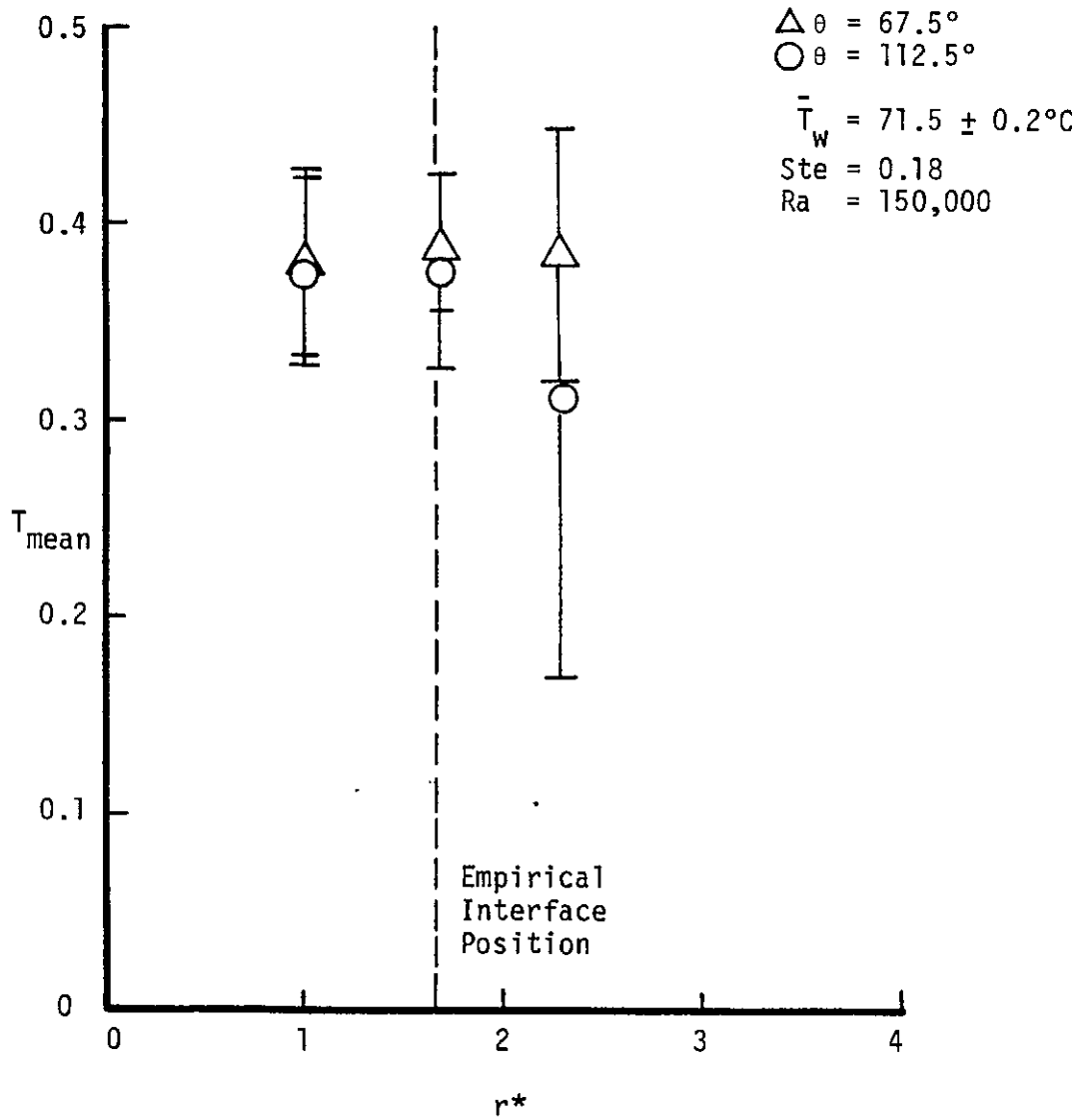


Fig. 4.8 Comparison of temperature along lines of constant θ to show symmetry, $t = 4.22$

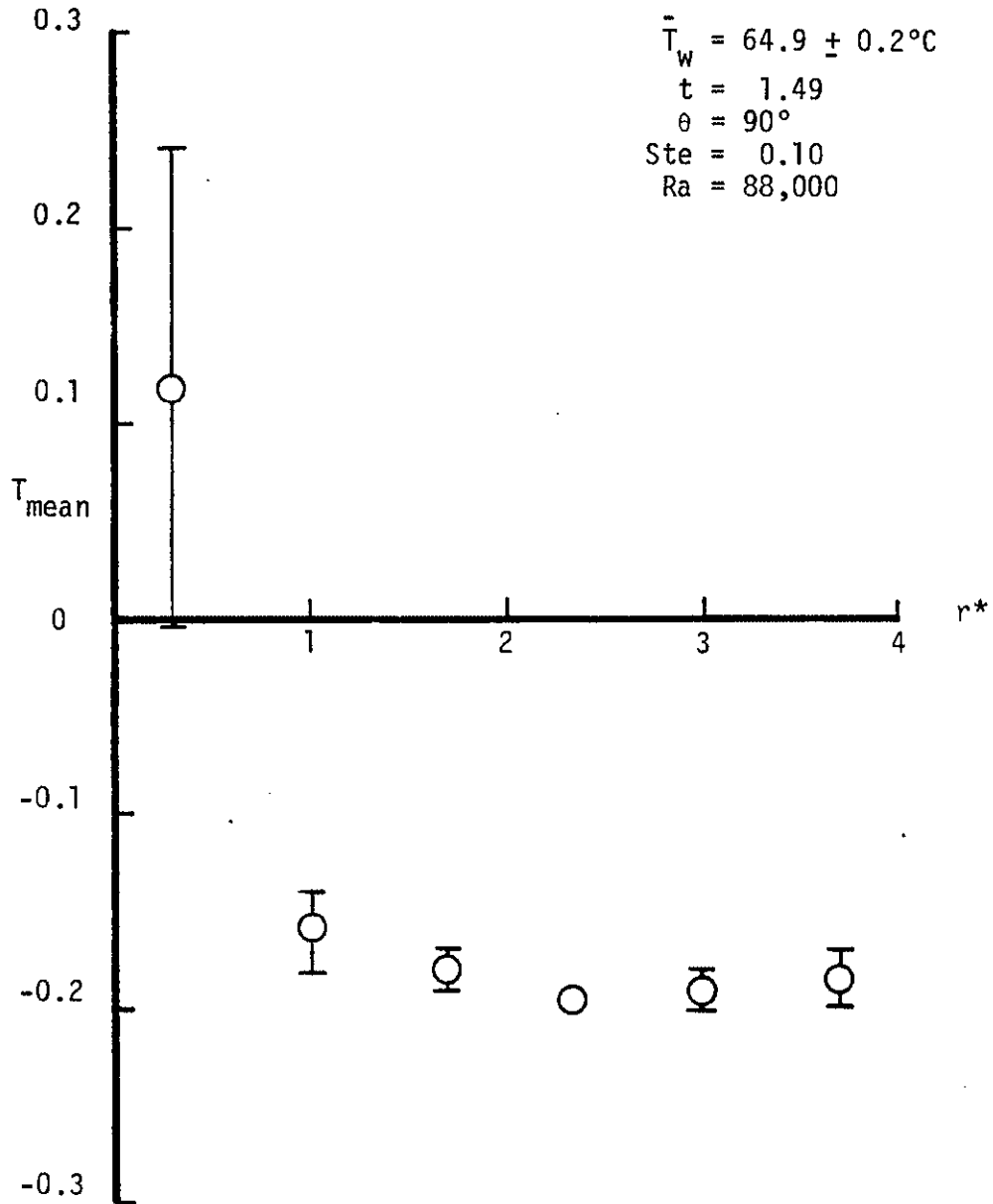


Fig. 4.9 Temperature along line $\theta = 90^\circ$, $t = 1.49$

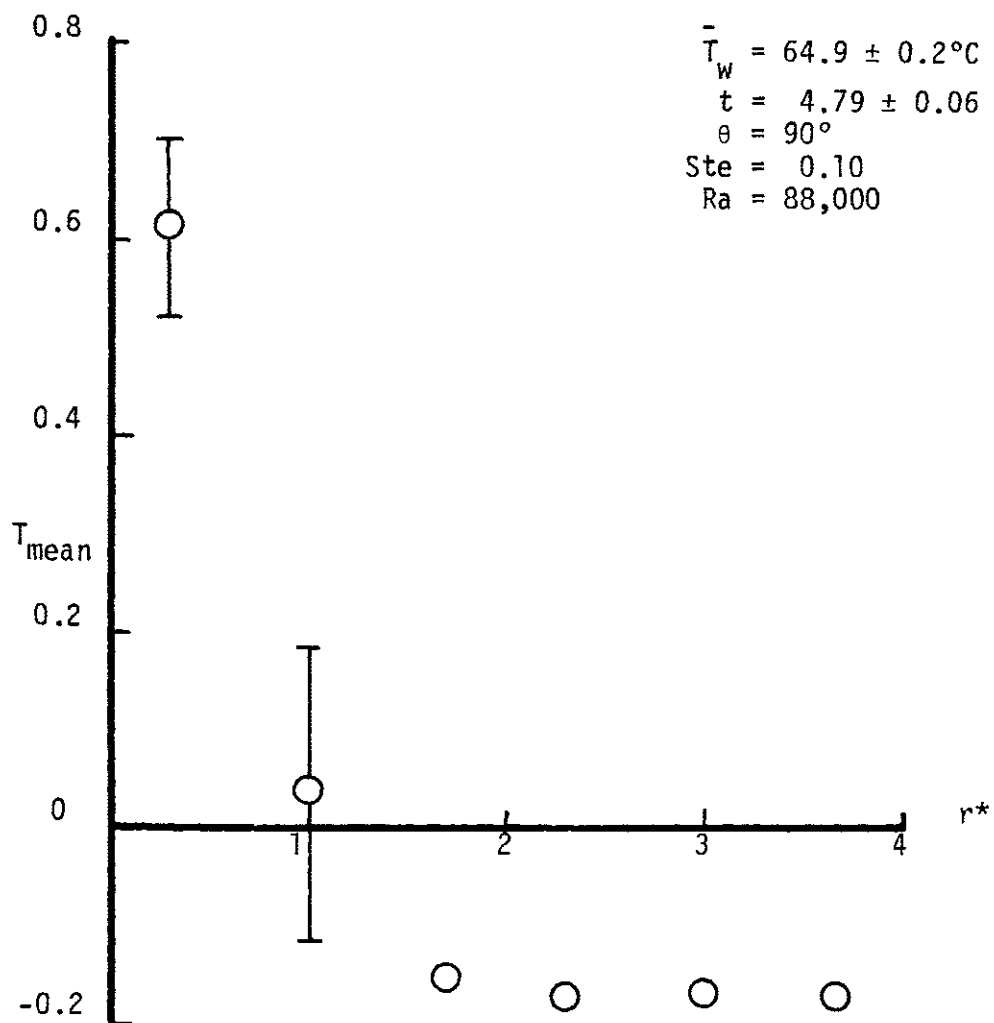


Fig. 4.10 Temperature along line $\theta = 90^\circ$, $t = 4.79$

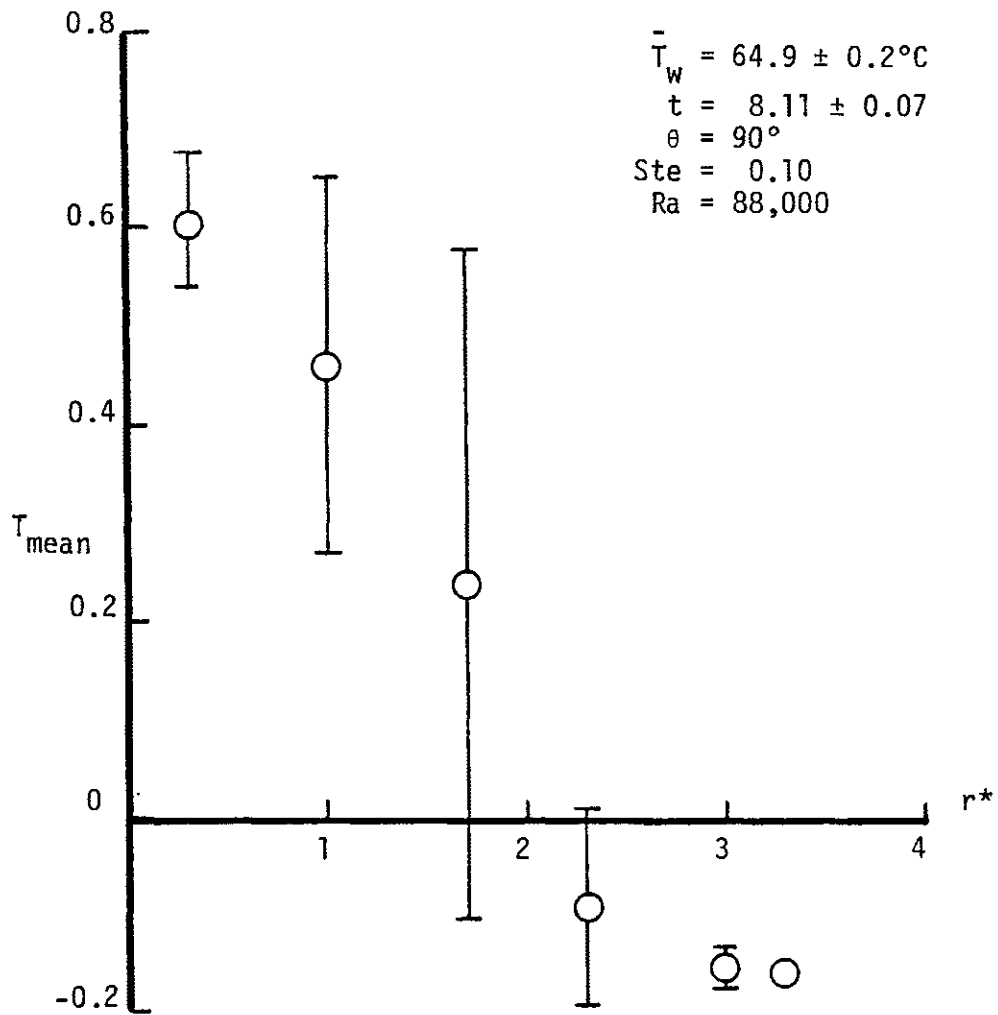


Fig. 4.11 Temperature along line $\theta = 90^\circ$, $t = 8.11$

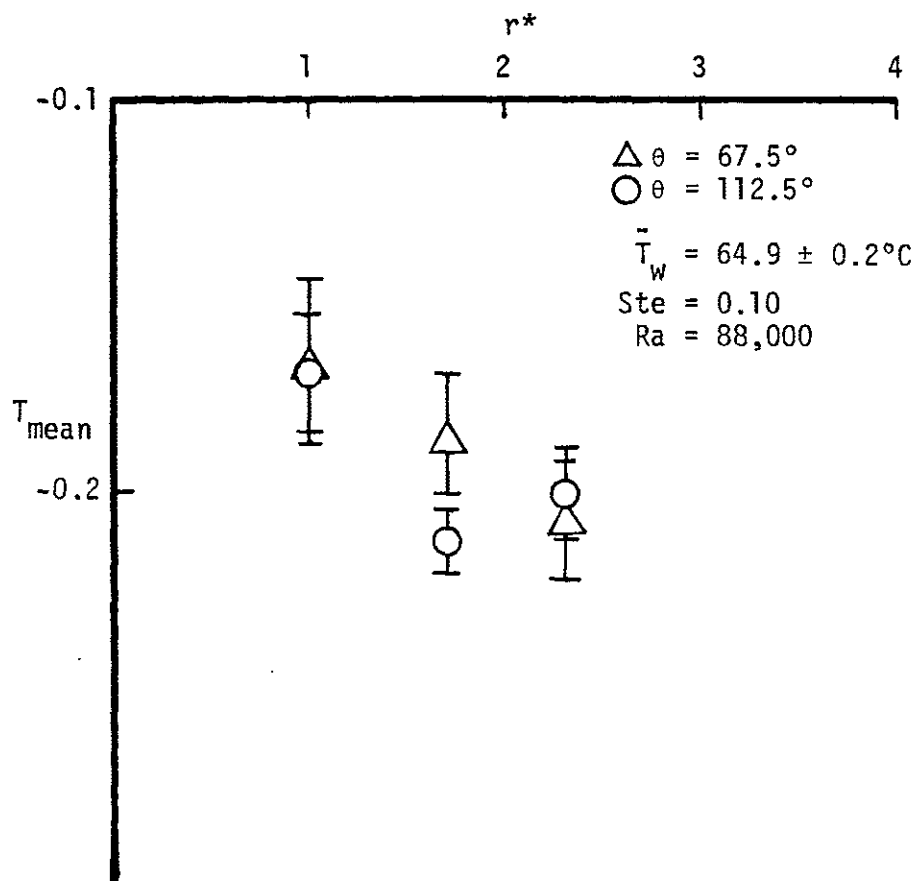


Fig. 4.12 Comparison of temperature along lines of constant θ to show symmetry, $t = 1.49$

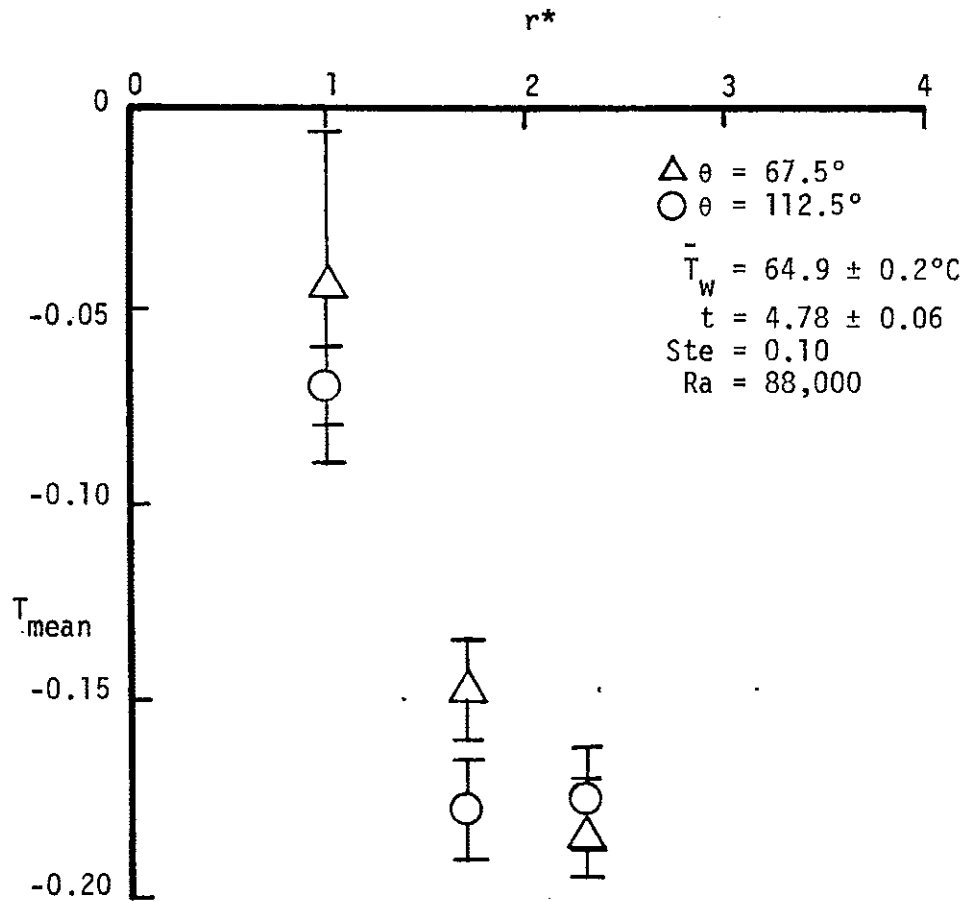


Fig. 4.13 Comparison of temperature along line of constant θ to show symmetry, $t = 4.78$

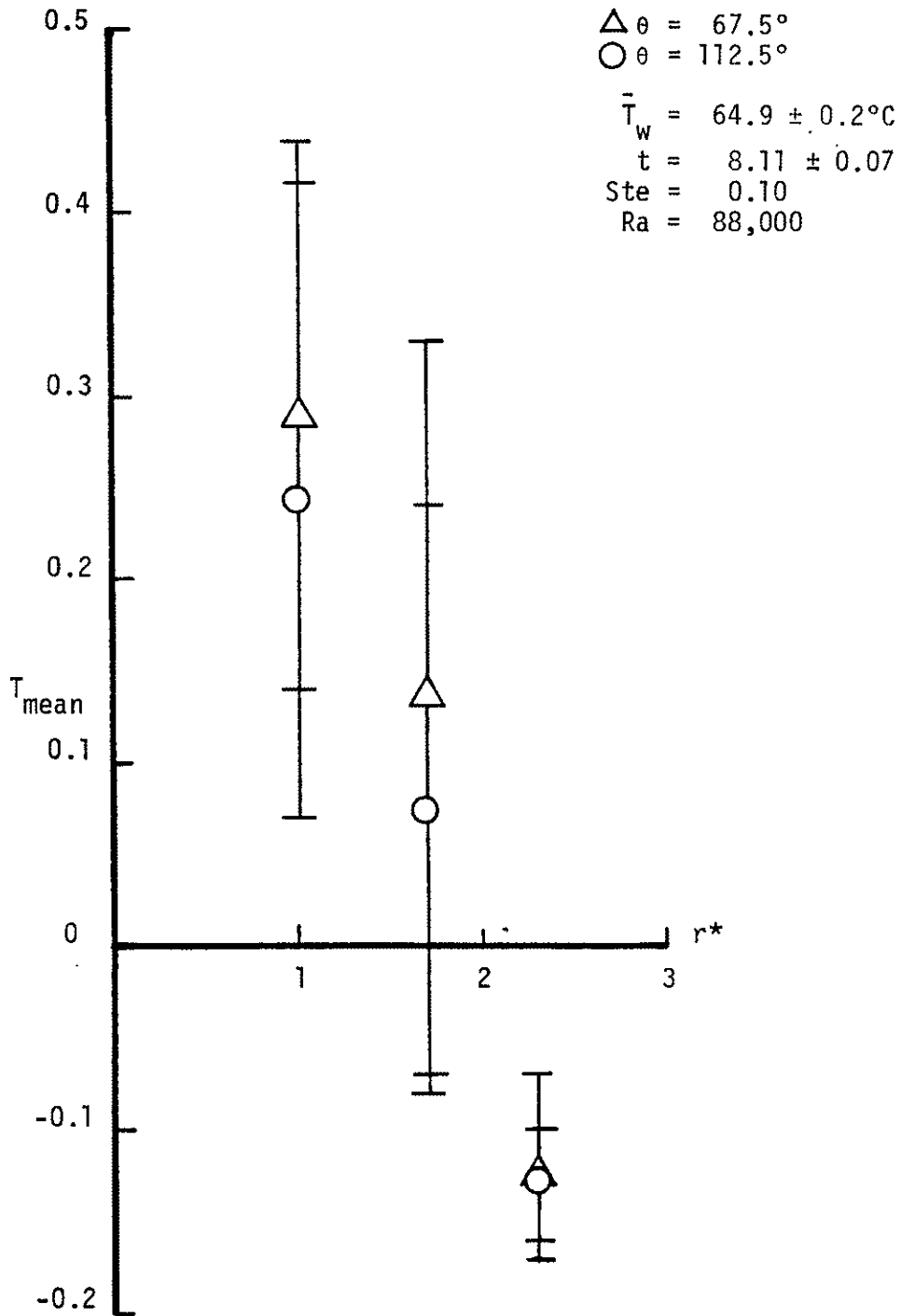


Fig. 4.14 Comparison of temperature along lines of constant θ to show symmetry, $t = 8.11$

Figures 4.15 through 4.17 show how the nondimensional temperature varies with time at three points. i.e, fixed (r, θ) on the mid-plane of the test cell. Shown on each graph is an experimental curve at one point for both sets of dimensionless parameters.

Figure 4.16 shows the temperature variation for $r^* = 0.33$ and $\theta = 90^\circ$ (symmetry plane). The shorter curve is for the larger set of parameters. This graph shows that the change in the temperature for the higher set of parameters is large at first. The temperature then reaches a maximum, oscillates for a period and continues oscillating as it drops off slightly. The lower set of parameters shows a similar trend. The temperature rises to a maximum and then oscillates slightly once the interface has passed this r^* location. The sharper rise in temperature for the higher set of parameters is due to the larger rate of energy addition to the system because of the higher cylinder wall temperature, resulting in a faster moving interface.

The standard deviations for the larger set of parameters become large after the temperatures start to rise and remain large until the temperatures start to drop off, oscillating slightly during the entire process. The standard deviations for the lower set of parameters are also large during the rise, but start to decrease just before the maximum is reached. When the maximum is reached, there is a small increase in the standard deviation that quickly disappears.

Figures 4.16 and 4.17 show the temperature variation for $r^* = 1.67$ and $r^* = 3.67$, with $\theta = 90^\circ$ (symmetry plane). Figure 4.16 shows that the temperature variation, for the higher set of parameters, follows the same trends shown in Fig. 4.15. It also shows that these

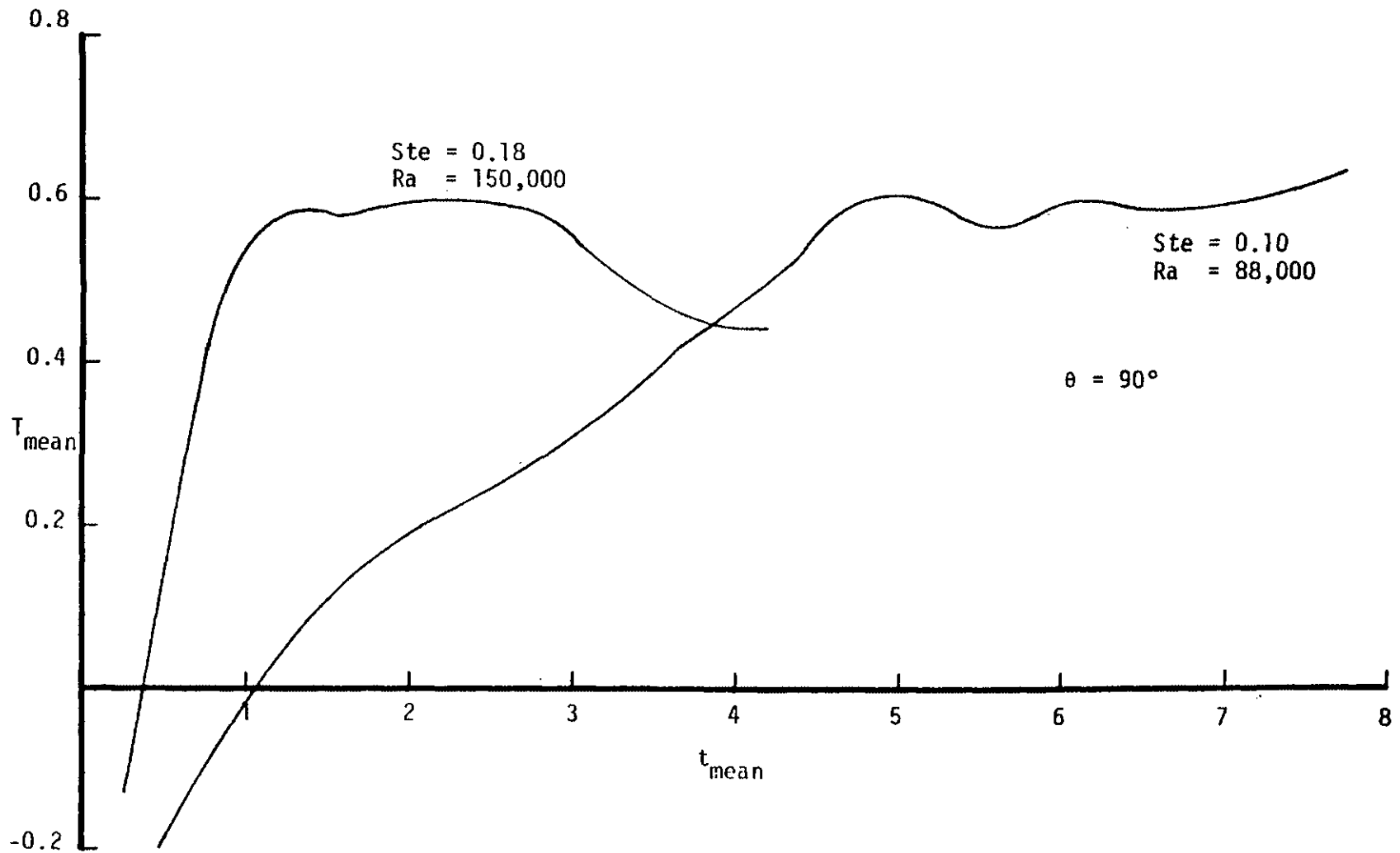


Fig. 4.15 Temperature variation with time, $r^* = 0.33$

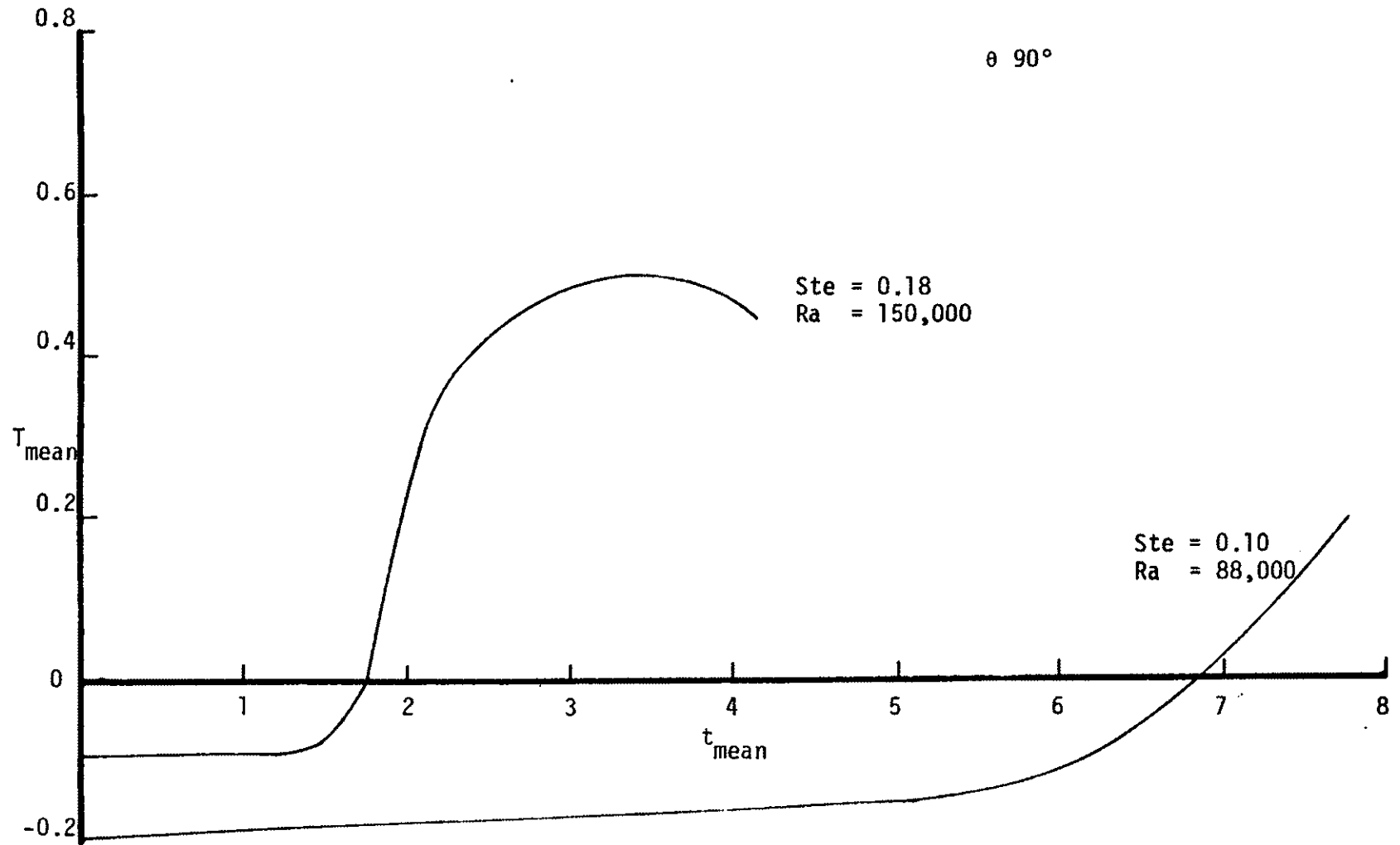


Fig. 4.16 Temperature variation with time, $r^* = 1.67$

trends hold for the lower set of parameters too (at least for the data available). The only conclusion that Fig. 4.17 allows is that the interface does not reach this point for the present experiments. The slight oscillation in the temperature at this point is probably due to the point's close proximity to the outer cell boundary and the varying environmental temperature ($\pm 2.2^\circ\text{C}$ or 4.0°F).

4.2 Discussion of Errors

This section discusses the errors or differences associated with the results presented in the first section of this chapter. The errors or differences are discussed in the same order as the results were presented.

4.2.1 Error in the Properties

The density was measured as described in Chap. 3 and earlier in this chapter. The volume of the weight used in this experiment was known to $\pm 1.0\%$ and the mass was known to ± 0.1 gram. Using standard error analysis [20], the error is found to be equal to the square root of two times the quantity, the uncertainty in the masses divided by the difference of the mass in the air and the mass in the paraffin quantity squared, plus the uncertainty in the volume divided by the volume quantity squared $(2 (\frac{\Delta m}{m_a - m_p})^2 + (\frac{\Delta V}{V})^2)^{1/2}$. The calculated error in the density measurement was found to be 1.1 %. This data agrees within 1% of the value reported for P-116 by Haji-Sheikh et al. [16], (see Table 4.2).

The error in the viscosity was calculated by taking the derivative of the Eq. (4.1). The error obtained by this method was 0.52% which is

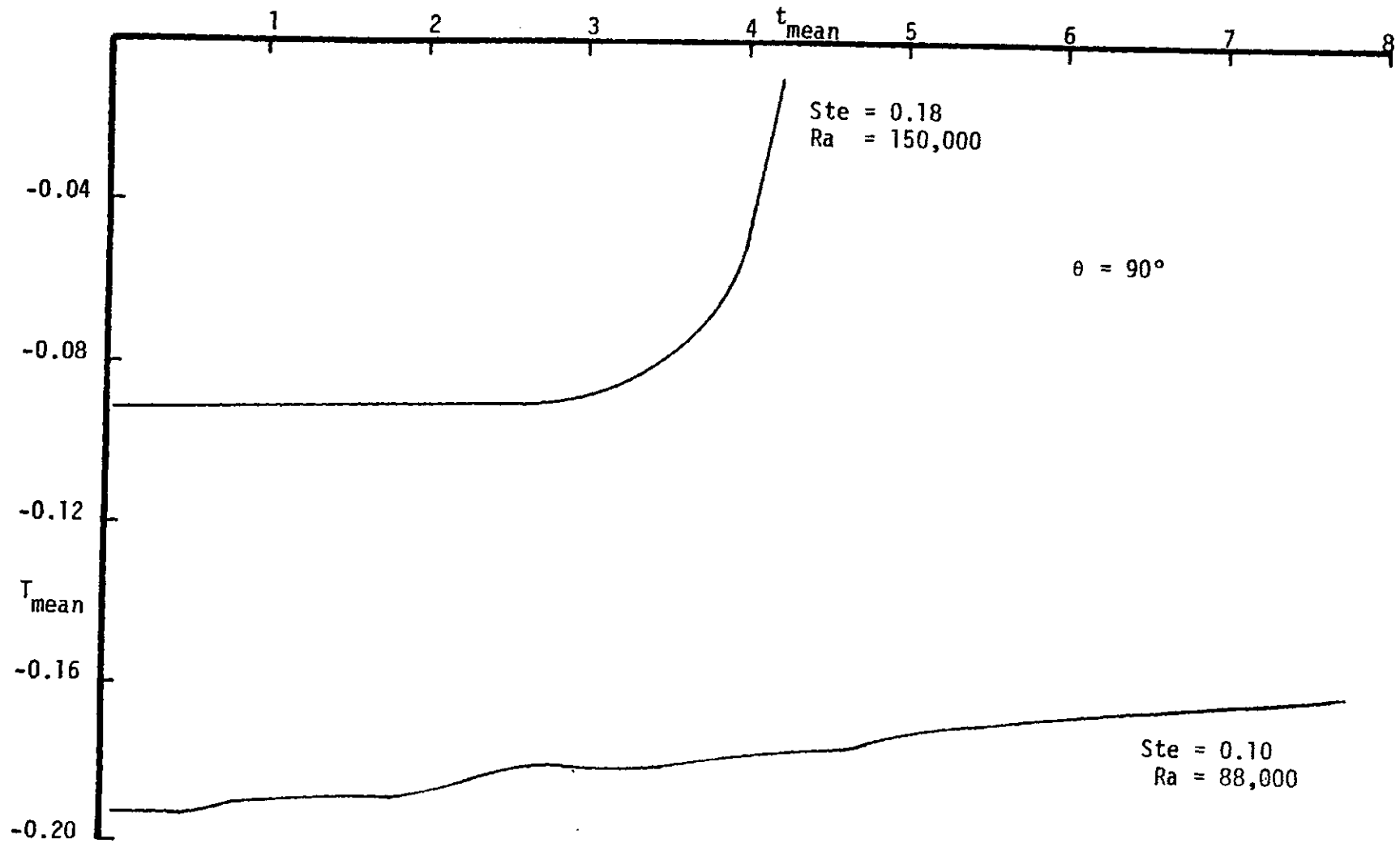


Fig. 4.17 Temperature variation with time, $r^* = 3.67$

smaller than the standard deviation of the data. Therefore, the standard deviation is a better measure of the reproducibility in the viscosity measurement (see Table 4.1). It should also be noted that this value is within 20% of the viscosity reported by Haji-Sheikh et al. [16] for P-116.

4.2.2 Error in the Interface Experiments

Three different interface experiments were undertaken. The three experiments are described in Chap. 3 and earlier in this chapter. The two experiments performed without thermocouples have the same error sources. The remaining experiment has one additional error source, the thermocouples which disturb the flow in the back half of the test cell. This error will be discussed in Sec. 4.2.3.

There are several sources of error in this experiment, although only three of these errors can be quantitatively reported. They are (1) the error in the controlled temperatures, (2) the error in the measurement of the interface position, and (3) the differences between interface positions for different data sets.

The above errors are all interrelated and therefore the error between the different sets of data contains the other errors also. In addition to the 2.5% (maximum) error, determined photographically, in the interface measurement, the 1% error in the cylinder temperature and the 5% error in the environmental temperature, there is one more major contributor to the difference between data sets. During the experiments gaseous bubbles appeared sporadically which disturbed the convectational flow patterns. The source of these bubbles is not known, but great care was taken to degas the paraffin in order to reduce or eliminate them.

The maximum differences between data sets ranged from 10% to 25%, i.e., interface position at fixed θ and since this difference includes all of the other error sources the maximum total error is 25%.

4.2.3 Error in the Temperature Measurements

The temperature was measured throughout the paraffin as described in Chaps. 3 and 4. Iron-constantan thermocouples have a maximum error of 2.2°C (4.0°F) as specified by the manufacturer. The thermocouples used in this experiment were calibrated at both the ice point and the boiling point of water. The maximum error at these points (which bound the temperature range of these experiments) was $\pm 0.40^{\circ}\text{C}$ (0.65°F) (see Table 4.4).

The temperatures reported in this thesis have been averaged and nondimensionalized. The dimensionless standard deviations have also been calculated and are shown in lieu of error bars on the graphs. These standard deviations are shown because they give a much better measure of the reproducibility of the experiments.

Finally, the effect of the thermocouples on the melt field must be discussed. As mentioned before the effect of the thermocouples was determined by comparing the interface position in a run with thermocouples to one without thermocouples. When this was done the interface position with thermocouples installed was within 10% of that found in the runs without thermocouples for the first half or 50 minutes of the experiment. After this time a bulge appeared in the interface near the top when the thermocouples were in place. This bulge varied in size starting out small and becoming larger at the end of the experiment (see Table 4.5). It should be noted that this bulge was not symmetric along the z axis. In the back half of the test cell where the

Table 4.4 Thermocouple calibration data*

Thermocouple Number	Temperature at ice point °C	Temperature at boiling point °C
0	0.1	100.4
1	0.1	100.4
3	0.1	100.3
4	0.2	100.3
5	0.2	100.3
10	-0.1	100.1
11	-0.1	100.1
12	-0.1	100.1
13	0.0	99.9
14	0.0	100.1
15	0.1	100.1
16	0.0	99.9
17	0.1	100.0
18	0.1	100.2
19	0.1	100.4
20	-0.1	100.1
21	0.0	100.2
22	-0.1	99.8
23	0.1	100.1
24	0.1	99.9
25	0.1	100.2
26	0.1	99.7
27	0.1	100.1
28	0.2	99.9
29	0.1	100.1

*Note: Although thermocouples 6,7,8 and 9 were calibrated previously their values are not shown here because they were being used to control the experiment when this calibration was done. Thermocouple number 2 was reading open.

thermocouple wires were located it appeared as though the interface was closer to the cylinder than it was when the thermocouples were not inserted. The probable cause of this z axis asymmetry is that the thermocouple wires obstruct the convective flow in the back half of the test cell which would cause a slower moving interface. Although these results may cause some doubt about the temperature measurements at later

times, they do show that the first 60% or more of the experiment still lies within the expected experimental error.

Table 4.5 Extent of interface misalignment comparing experiments with and without thermocouples*

Time (minutes)	Location of Misalignment	Maximum difference between Interface radii
60	40° to 110°	21%
70	40° to 140°	44%
80	30° to 140°	61%
90	40° to 140°	58%
100	30° to 150°	68%

*Note: the maximum difference between interface radii for 60 minutes is within the expected experimental error, $\approx 25\%$.

Chapter 5

COMPARISON OF RESULTS WITH THEORY

The results of the current experiments are compared with the numerical results of Prusa and Yao [11] in this chapter. The comparisons are made in two parts. The first part compares the results obtained in the interface experiments with theory. The second part compares the results of the temperature experiments with theory.

5.1 Interface Results Comparisons

Figures 5.1 and 5.2 show a comparison in the interface extrema (i.e. vertical top $\theta = 90^\circ$ and bottom $\theta = 90^\circ$) between the current work and the results of [11]. Figure 5.1 shows the comparison at $\theta = -90^\circ$, this graph shows that the data for both sets of dimensionless parameters lies below the theoretical curve of [11]. This was expected for two reasons. First, the theoretical curve does not contain any of the error sources of the experimental data. Second, even though the Rayleigh numbers are much larger for the data, their effects are much more prevalent at the top of the melt region than at the bottom of the cylinder, and are therefore outweighed by the error sources.

Figure 5.2 shows a comparison of the interface position at $\theta = 90^\circ$ (vertical top) using the current data and the theory of Prusa and Yao [11]. The data for the larger set of Stefan and Rayleigh numbers lies above the theoretical curve of [11]. This is not surprising because both parameters are larger than the parameters for

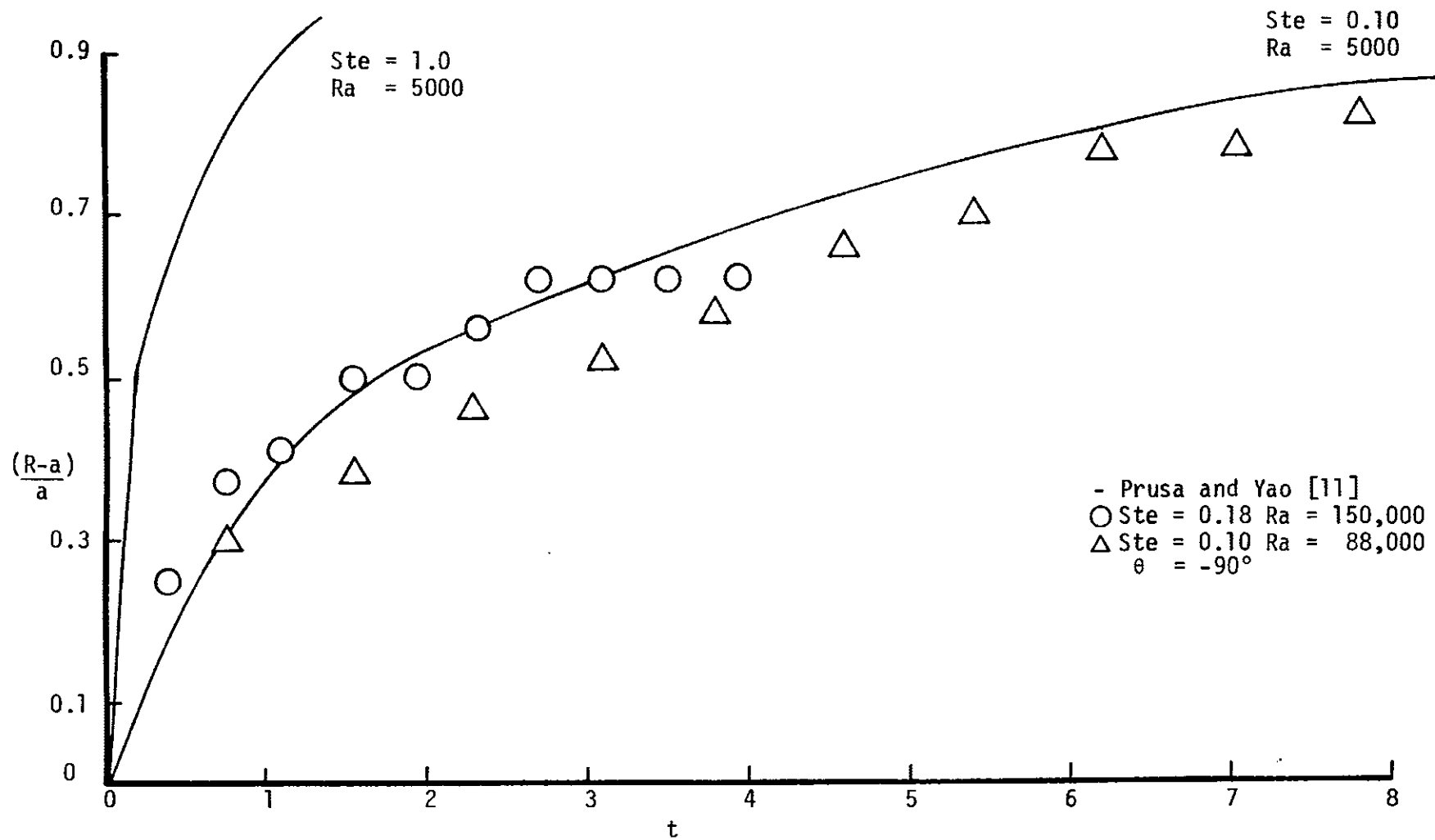


Fig. 5.1 Comparison of interface minimum

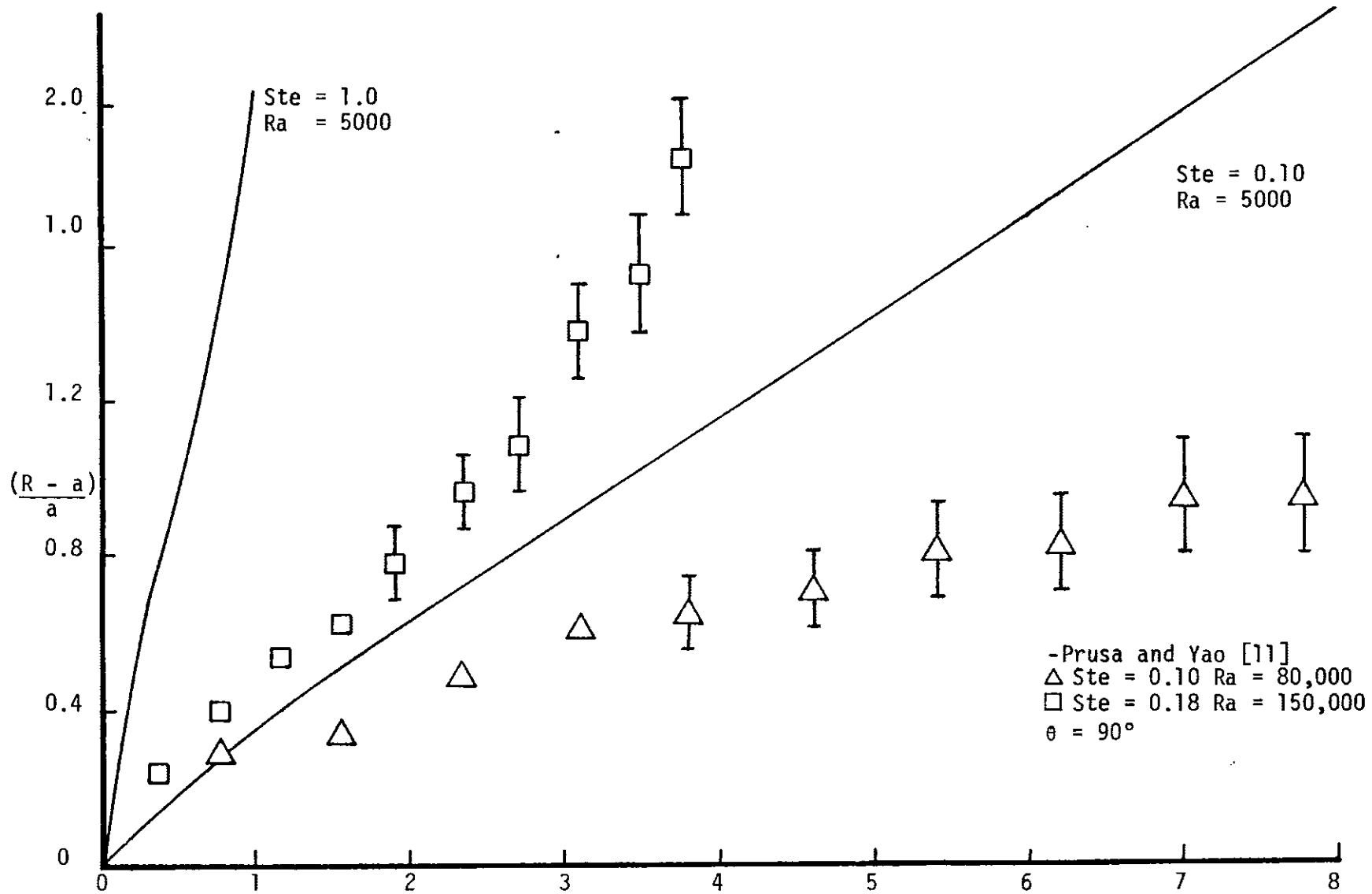


Fig. 5.2 Comparison of Interface maximum

the theoretical curve. Also, the effect of the Rayleigh number is dominant in the upper part of the melt region (especially at later times). The data for the smaller set of parameters lies just below the theoretical curve. At first, this may seem surprising because the experimental Rayleigh number is so much larger but considering that the Stefan number is the same and there is up to a 25% error in the interface position, the agreement may be within experimental error.

A comparison between the theoretical and the experimental dimensionless melt volumes is shown in Fig. 5.3. Prusa and Yao [11] concluded that the Stefan number was the controlling parameter in determining the melt volume, and that the Rayleigh number does not effect the melt volume until later times. The graph in Fig. 5.3 supports these conclusions. The experimental data and the theoretical curves shown on this graph are at similar Stefan numbers but the Rayleigh numbers for the experiments are an order of magnitude larger. Yet, the trends for both the experimental data and the theoretical curves are the same for the data shown. The experimental data for $Ste. = 0.18$ lies just above the theoretical curve for $Ste = 0.10$. This shows that there is a larger melt zone for the larger Stefan number, just as expected. The data for $Ste = 0.10$ lies below the theoretical curve for the same Stefan number, which may again be due to the degree of experimental uncertainty.

5.2 Temperature Results Comparisons

Two comparisons are made between the measured temperatures and the temperatures calculated by Prusa and Yao [11]. The first comparison is

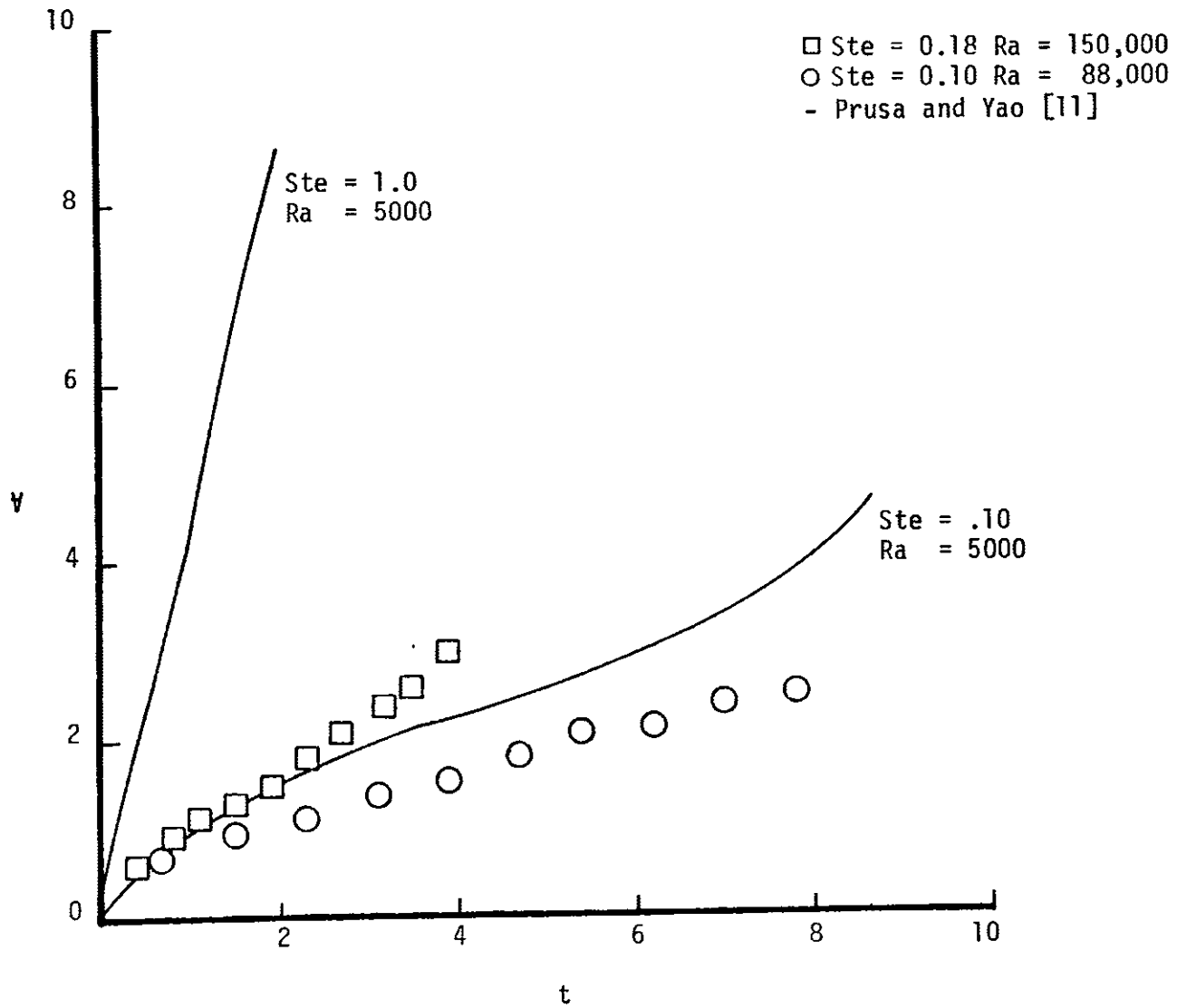


Fig. 5.3 Comparison of melt volumes

shown in Figs. 5.4 and 5.5 and is a comparison of the temperatures along the line $\theta = 90^\circ$ (vertical top) at two times.

Figure 5.4 shows the comparison of the theoretical curve at $t = 1.75$ and the experimental data at $t = 1.82$. The Stefan numbers are the same ($Ste = 0.10$). The Rayleigh number for the experimental data was 88,000 while it was 5000 for the theoretical curve. The scale for the theoretical curve was determined by estimating the interface position based on the mean temperatures. Since only one data point was available in the melt, little can be said about this comparison except that the trends agree. The experimental data point does lie below the theoretical curve which may yet be due to experimental error.

Figure 5.5 shows the comparison of the same dimensionless parameters at $t = 8.8$ for the theoretical curve and $t = 8.11 \pm 0.07$ for the experimental data. The scale for the theoretical curve, once again, was determined by estimating the interface position using the mean temperatures found in several experimental runs. If the top part of the error bars shown on this graph were connected, the experimental data would show a similar shape to the shape of the theoretical curve. Once again, the experimental data lies below the theoretical curve.

The second comparison is shown in Fig. 5.6, where contrast is made between isothermal contours. Figure 5.6A shows the isotherms calculated by Prusa and Yao [11] at $t = 8.8$. The isotherms shown in Fig. 5.6B are from the experiments $t = 8.11 \pm 0.07$, and were drawn while trying to reproduce a similar pattern to that of Fig. 5.6A. This was done by determining the temperature range of each thermocouple. The temperature at each thermocouple location was then taken as the value,

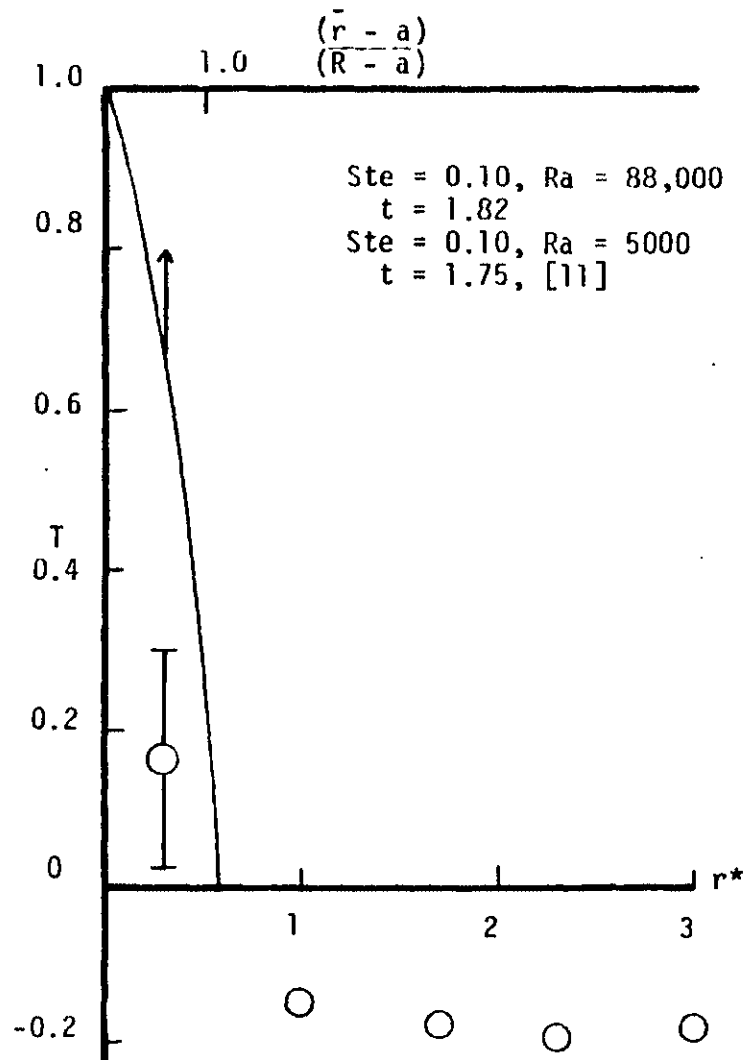


Fig. 5.4 Comparison of temperatures along line $\theta = 90^\circ$ at an early time

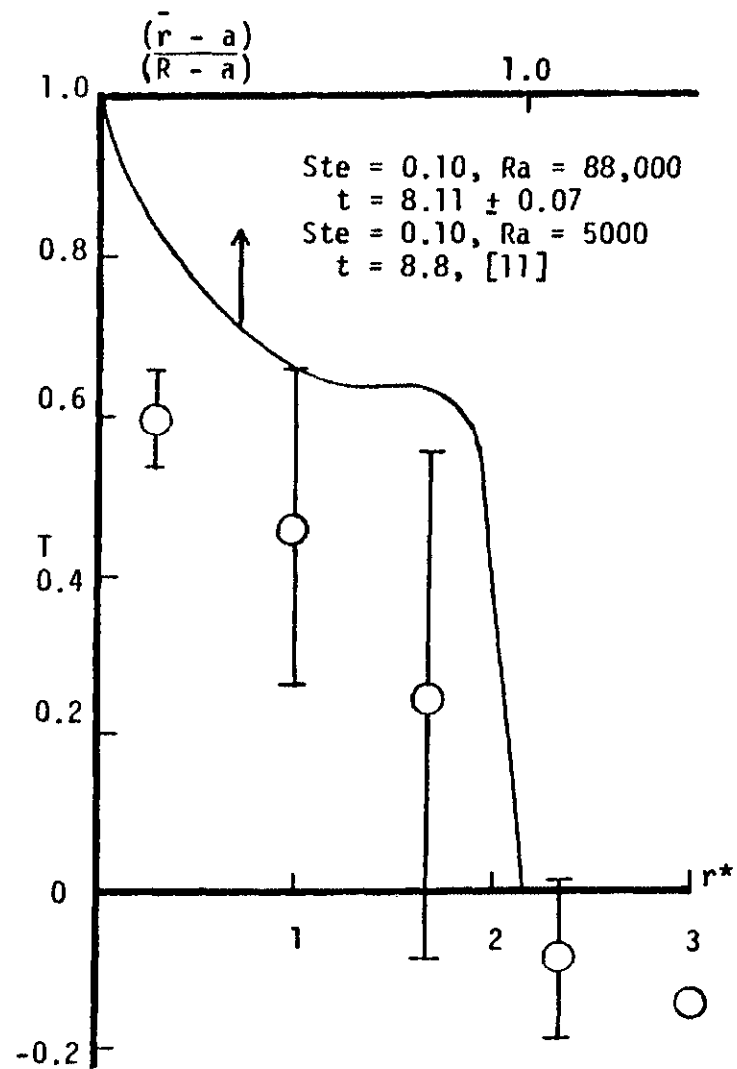


Fig. 5.5 Comparison of temperature along line $\theta = 90^\circ$ at a late time

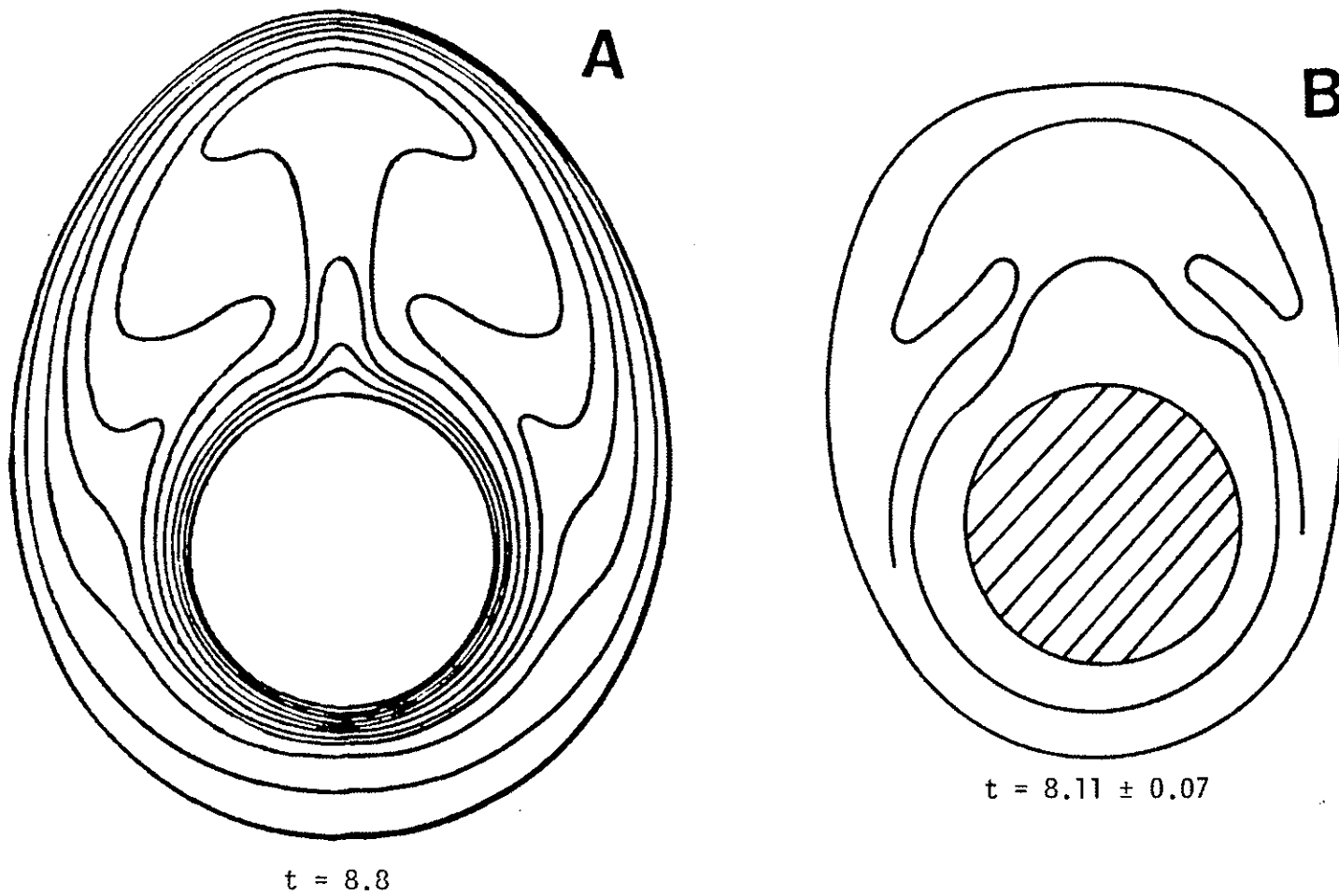


Fig. 5.6 Isotherm comparison

within these ranges, which most closely reproduced the symmetries of the isotherms of Fig. 5.6 A (see Table 5.1 for the temperature ranges). These temperature ranges were given by one standard deviation either side of the mean temperature. This comparison is a semi-quantitative representation of the temperature field. It shows that the predicted isotherms are reasonable and could quite possibly be confirmed if a more detailed experimental temperature field could be measured.

Table 5.1 Temperature ranges used to
develop the experimental isotherms*

Thermocouple Number	Nondimensional Temperature Range	Mean Nondimensional Temperature
0	.3700 to .4100	.3900
1	.3012 to .4504	.3758
3	.2719 to .3155	.2937
4	.3529 to .4533	.4031
5	.4866 to .5180	.5023
10	.3688 to .3914	.3801
11	.5487 to .6641	.6064
12	.0505 to .2185	.1345
13	.1368 to .4440	.2904
14	.2651 to .6553	.4602
16	-.0019 to .237	.1177
18	-.0704 to .3472	.1384
19	-.2030 to .5856	.2413
20	-.0917 to .2419	.0751
23	-.1952 to .0196	-.0878

*Note: Thermocouple number 2 was reading open. $Fo = 8.11 \pm .07$.

Chapter 6

CONCLUSIONS AND RECOMMENDATIONS

The information obtained in these experiments has added to the data base available on melting around an isothermal horizontal cylinder. The error in these results has been presented in terms of the ability to reproduce experimental results. The reproducibility of these experiments is very good at early times but seems to deteriorate with time. This data has been compared favorably with the numerical results, computed from the model of Prusa and Yao [11]. These comparisons seem to support the numerical solution proposed by those authors, and show that their model is well conceived. Unfortunately, these experiments do not prove conclusively that the numerical analysis of [11] is correct. Closer correlation may be achieved by performing several experiments where the nondimensional parameters are the same as those reported in the analysis by Prusa and Yao [11]. The experiments should include measurements of the interface position and temperature field, as done in the current experiments, along with velocity field and Nusselt number measurements. To increase the reproducibility of the experiments it is recommended that better controls be used on the cylinder and environmental temperatures. It is also recommended that both the temperature and velocity fields be measured nonobtrusively. There are several laser techniques that could be used to do this. If non-obtrusive temperature measurements cannot be made, type K (chromel-

alumel) or some other thermocouple wire not containing copper* should be used. It is also felt that using a pure paraffin would help to eliminate some of the experimental problems.

Finally, there is some evidence of a possible oscillation in the experimental flow field. This may be seen in the large error bars near the melting interface and the oscillation that shows up in the temperature variation at a single point (see Fig. 4.15). Transitional flow is a possibility at the relatively high Rayleigh numbers of these experiments. In any case, the author believes this evidence to be an indication of the difficulty in reproducing the exact experimental conditions from run to run. Additional research (both numerical and experimental) could determine if the flow field reaches transition, some eddy inception condition, and when this takes place. The velocity experiments mentioned earlier would be very useful in this determination.

*There is some evidence of a Cu-Paraffin chemical reaction

REFERENCES

1. Carslaw, H. S. and Jaeger, J. C., Conduction of Heat in Solids, 2nd ed., Oxford Press, GB, Chap XI, 1959.
2. Hale, N. W., Jr. and Viskanta, R., "Solid-Liquid Phase-Change Heat Transfer and Interface Motion in Materials Cooled or Heated from Above or Below," International Journal of Heat and Mass Transfer, Pergamon Press Ltd., GB, Vol. 23, March 1980, page 283-292.
3. Hale, N. W., Jr. and Viskanta, R., "Photographic Observation of the Solid-Liquid Interface Motion During Melting of a Solid Heated from an Isothermal Vertical Wall," Letters in Heat Transfer, Vol. 5, Number 6, June 1978, pp. 329-337.
4. Bathelt, A. G., Viskanta, R. and Leidenfrost W., "Latent Heat-of-Fusion Energy Storage: Experiments on Heat Transfer from Cylinders During Melting," Journal of Heat Transfer, Vol. 101, August 1979, page 453-458.
5. Bathelt, A. G., Viskanta, R., and Leidenfrost, W., "An Experimental Investigation of Natural Convection in the Melted Region Around a Heated Horizontal Cylinder," Journal of Fluid Mechanics, Vol. 90, Part 2, January 1979, pp. 227-239.
6. Bathelt, A. G., Viskanta, R., and Leidenfrost, W., "Experiments on the Role of Natural Convection and Heat Source in the Melting of a Solid," ASME Heat Transfer Division Paper Number 78-HT-47, 1978.
7. Bathelt, A. G. and Viskanta, R., "Heat Transfer and Interface Motion During Melting and Solidification Around a Finned Heat Source Sink," ASME Heat Transfer Division Paper Number 80-HT-10, 1980.
8. Sparrow, E. M., Schmidt, R. A., and Ramsey, J. W., "Experiments on the Role of Natural Convection in the Melting of Solids," Journal of Heat Transfer, Vol. 100, February 1978, pp. 11-16.
9. Sparrow, E. M., Patankar, S. V., and Ramadhyani, S., "Analysis of Melting in the Presence of Natural Convection in the Melt Region," Journal of Heat Transfer, Vol. 99, November 1977, pp. 520-526.
10. Reiger, H., Projahn, U., and Beer, H., "Analysis of the Heat Transport Mechanisms During Melting Around a Horizontal Circular Cylinder," International Journal of Heat and Mass Transfer, Pergamon Press Ltd., GB, Vol. 25, Number 1, January 1982, pp. 137-147.
11. Prusa, J. and Yao, L. S., "Melting Around a Horizontal Heated Cylinder: Part I - Numerical Solution for Isothermal Boundary Condition," Joint ASME/JSME Thermal Engineering Conference, March 20-23, 1983 Honolulu, Hawaii.

12. Bathelt, A. G., Van Buren, P. D., and Viskanta, R., "Heat Transfer During Solidification Around a Cooled Horizontal Cylinder," AICHE Symposium Series Heat Transfer, 1979, San Diego, California.
13. Sparrow, E. M., Ramsey, J. W., and Kemink, R. G., "Freezing Controlled by Natural Convection," Journal of Heat Transfer, Vol. 101, November 1979, pp. 578-584.
14. Sparrow, E. M., Ramsey, J. W., and Harris, J. S., "The Transition from Natural Convection Controlled Freezing to Conduction Controlled Freezing," Journal of Heat Transfer, Vol. 103, February 1981, pp. 7-12.
15. Kays, W. M. and Crawford, M. C., Convective Heat and Mass Transfer 2nd ed. McGraw-Hill Book Company, New York, 1980.
16. Haji-Sheikh, Eftekhar, J., and Lou, D. Y. S., "Some Thermophysical Properties of Paraffin Wax As A Thermal Storage Medium," Joint AIAA/ASME Thermophysical Conference, June 7-11, 1982, St. Louis, Missouri.
17. Stenger, R. J., Manager, Wax Technology, Suntech Group, Personal communication, 1982.
18. Born, M. and Wolf, E., Principles of Optics Electromagnetic Theory of Propagation Interface and Diffraction of Light, Pergamon Press, GB, Chap. 1, 1970.
19. Baumeister, T., Avallone, E. A., and Baumeister, T., III, Editors, Mark's Standard Handbook for Mechanical Engineers, 8th ed., McGraw-Hill Book Company, New York, Chap. 3, 1978.
20. Holman, J. P., Experimental Methods for Engineers, 2nd ed., McGraw-Hill Book Company, New York, Chap. 3, 1971.

APPENDIX A

PROGRAM LISTING FOR DATA AQUISITION

```

10  !THIS PROGRAM TAKES TEMPERATURE DATA WHEN CONNECTED VIA HP-IB BUS
    TO THE FLUKE 2200B DATA
20  ! LOGGER
30  DIM T$(950), R(49, 29)
40  K = 1
50  DISP "What is time increment between data runs in minutes"
60  INPUT Q
70  DISP "What is the new temp file name"
80  INPUT Z$
90  DISP "What is the new time file name"
100 INPUT Y$
110 CREATE Z$, 47
120 ASSIGN# 1 to Z$
130 DISP "TO START TAKING DATA HIT CONT"
140 PAUSE
150 FOR I = 0 TO 49
160 L = 0
170 ! Next 4 lines look for last channel
180 TRIGGER 7
190 ENTER 700, A$
200 IF A$[3,4] = "29" THEN 230
210 GOTO 180
220 ! This loop takes the data and records the time
230 FOR J = 1 TO 33
240 TRIGGER 7
250 ENTER 700, A$
260 IF A$[1,1]= "Y" THEN 320
270 C = VAL (A$[3,4])
280 R(I,C) = VAL(A$[8,12])
290 PRINT # 1, R(I,C)
300 IF C = 29 THEN J = 33
310 GOTO 370
320 IF L>=1 THEN 350
330 T$[K, K+9]=A$[6,13]
340 K=K+9
350 L=L+1
360 B$=A$
370 NEXT J
380 RESET 7
390 WAIT Q * 60000
400 NEXT I
410 ! The next step displays the time matrix
420 DISP T$
430 ! The next step displays the temperature matrix
440 MAT DISP R;
450 ASSIGN# 1 TO *
460 CREATE Y$, 4
470 ASSIGN# 2 TO Y$

```

```
480 PRINT#2; T$
490 ASSIGN# 2 TO *
500 DISP "DATA TAKING IS COMPLETE"
510 DISP "TO USE DATA TYPE ASSIGN# (PLACE BUFFER NUMBER HERE W/O
BRACKETS) TO FILE NAME"
520 DISP "THEN TYPE READ# BUFFER NUMBER; VARIABLE"
530 END
```

APPENDIX B

COMPOSITION OF P-127 PARAFFIN

Paraffin	fraction
C ₂₁ H ₄₄	0.35%
C ₂₂ H ₄₆	1.86%
C ₂₃ H ₄₈	6.50%
C ₂₄ H ₅₀	13.04%
C ₂₅ H ₅₂	16.38%
C ₂₆ H ₅₄	16.30%
C ₂₇ H ₅₆	12.70%
C ₂₈ H ₅₈	9.50%
C ₂₉ H ₆₀	6.30%
C ₃₀ H ₆₂	3.60%
C ₃₁ H ₆₄	2.10%
C ₃₂ H ₆₆	1.10%
C ₃₃ H ₆₈	0.50%
C ₃₄ H ₇₀	0.30%
Isoparaffins	9.47%

This information was obtained from Reference [17].

APPENDIX C
INSTRUMENT SERIAL NUMBERS

Instrument	Serial Number
Fluke 2200B Data logger	2220010
HP-85 Micro-computer	2213A62827
HP-IB 82937A Interface	82937-60004
LAUDA Model T-1 constant Temperature Bath	B02002
Power Designs Inc. Power Supply Model 4005	J403153

A10600 093799

OLD DOMINION UNIVERSITY LIBRARY
LD4331.E53R652
Experiments on melting around an isother



3 9356 002165505

LD 433.1 .E53 R652

Rothgeb, Timothy Moore.

Experiments on melting
around an isothermal